# Studies of oscillator neural networks modeling the time correlation of neuronal spikes

NOMURA Masaki

## Abstract

We study a simple extended model of oscillator neural networks concerning the associative memory with sparsely coded phase patterns, in which information is encoded both in the mean activity level and in the timing of spikes. In this model, we treat sparse coding and temporal coding at the same time. We adopted the theory of statistical neurodynamics to investigate the order parameter equations governing both the equilibrium state and the retrieving process.

At first, we study the basic properties of the auto-associative memory. Applying the methods of statistical neurodynamics to our model, we theoretically investigate the model's associative memory capability by evaluating its maximum storage capacities and deriving its basins of attraction. We found that the maximum storage capacity diverges in the sparse coding limit and the basin of attraction remains large even just below the maximum storage capacity. Our theoretical results are in good accordance with those of numerical simulations. Then, we consider the association of sequential patterns and that of patterns with different activity levels. We also found that the basin of attraction can be enhanced by introducing the dynamically adjusted threshold. Furthermore, the robustness against random synaptic dilution are also studied. It is found that even in the case of a high cutting rate, the basin of attraction remains large and the maximum storage capacity still diverges in the sparse coding limit.

It is known that the mixed state plays significant roles in the information processing. Thus, second, we study the stability of mixed states in oscillator neural networks, where we choose correlated patterns to be embedded. Applying the theory of statistical neuro dynamics to our model, we estimate the maximum storage capacity with respect to the OR mixed state, which is composed of correlated patterns. We found that the maximum storage capacity diverges in the sparse coding limit. The results are supported by numer-

ical simulation. In addition, we consider the stability of another type of mixed state by numerical simulation. The result suggests that the latter type of mixed state is less stable than the OR mixed state. This feature is the result of the dual coding system and is not seen in binary models. The difference of the stability between these mixed states suggests importance of introducing the timing of neuronal spikes into the information processing.



## Acknowledgment

The author would like to express his sincere gratitude to Professor Toyonori Munakata for his guidance and discussion. He is also grateful to Associate Professor Akito Igarashi and Lecturer Toshio Aoyagi for valuable discussions, encouragements and critically reading the manuscript.

He would like to express his deep gratitude to his parent for her continual support and encouragement.

# Contents

# Chapter 1

# Introduction

## 1.1 Brief overviews of the Modeling Neural Networks

The brain processes many types of information and can be separated into many regions depending on their functions, such as the auditory system, the visual system and so on. Each system is composed of many modules which provide specific function. The brain, which is sometimes called the central nervous systems, is hierarchically structured. After the discovery of the electrical nature of the nervous signals by Galvani, Ramon y Cajal showed that the system is made of an assembly of cells which he called *neurons*. Now, the human brain is said to comprise approximately $3 \times 10^{10}$ neurons [1]. The neurons communicate each other through the synaptic connections (see Fig.1.1). One neuron receives signals from other neurons through synaptic connections. Then, the inputs are transmitted to the soma. At the soma, the inputs are summed up, and when the total voltage is enough high, a signal, called spike or action potential, is propagated through the axon. The generated spike is transmitted to the next neurons via synaptic connections.

McCulloch and Pitts studied the modeling of real neurons, in which they proposed *a formal neuron* including the properties mentioned above [2]. It is a binary unit which takes two internal states. The state of a unit is determined by the value resulted from the summation of the input signals. If it is larger than a threshold value, the unit is in

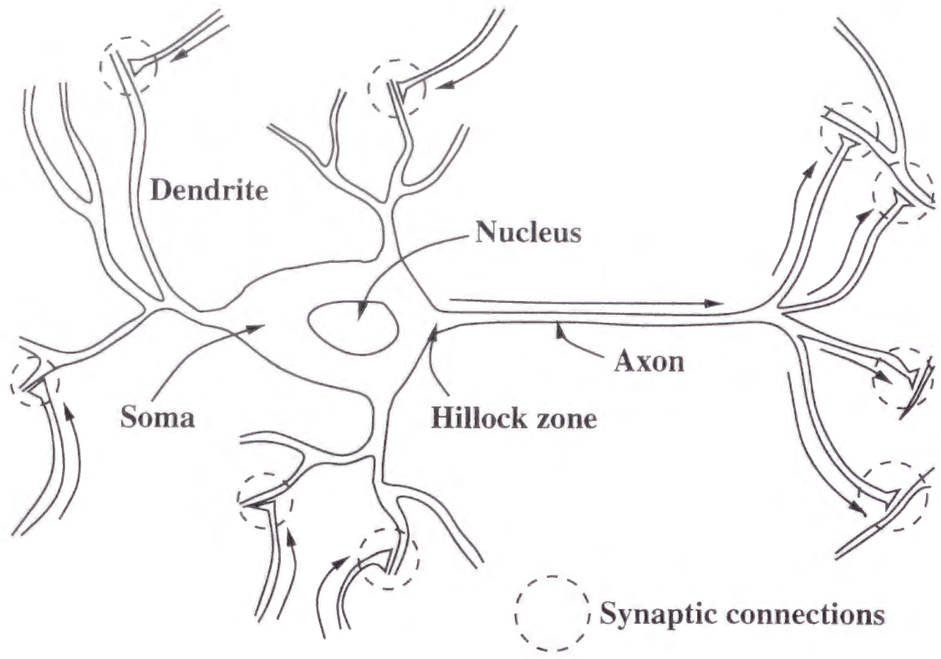


Figure 1.1: neuron

firing state, which corresponds to propagating the action potential. Otherwise, the unit is in non-firing state, where no action potentials are generated. When we represent the state of the $j$-th unit by $S_j$, where $S_j$ takes 1 for firing state and 0 for non-firing state, the state of the $i$-th unit is determined by

$$S_i = \Theta\left(\sum_j J_{ij} S_j - H_i\right), \tag{1.1}$$

where $J_{ij}$ corresponds to the synaptic efficacies in Fig.1.2, $H_i$ is a threshold value, and $\Theta(x)$ is a step function defined by

$$\Theta(x) = \begin{cases} 1 & \text{for } x \geq 0 \\ 0 & \text{for } x < 0. \end{cases} \tag{1.2}$$

Here, the summation is executed for all the sites linked to the $i$-th unit.

After their studies, Hopfield proposed a collective memory model with McCullo-Pitts neurons [3]. In this model, memory is considered to be the result of the interaction between



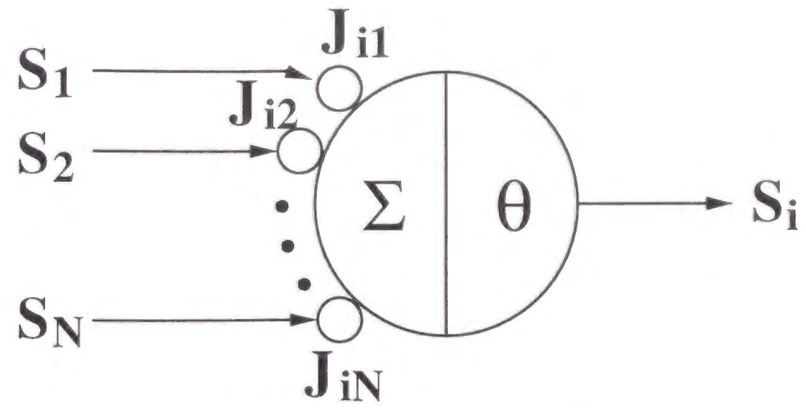


Figure 1.2: McCullo-Pitts neuron

a large number of formal neurons, and the memory is stored in the synaptic efficacies $J_{ij}$. He adopted a symmetric Hebb rule [4] as the synaptic efficacy. This rule is based on the hypothesis from the biological experiments that when the $i$-th and the $j$-th neurons are firing simultaneously, the connection between them is enhanced, and otherwise it is weakened. The most important aspect of the Hopfield model is its analogy to the spin glass model in statistical physics. He proved that his model has the Lyapnov function, and thus, the macroscopic behaviors of the model can be investigated by the theory of statistical physics. Indeed using the replica theory which is a method of statistical physics, Amit et al calculated that the storage capacity of the Hopfield model is 0.138 [5].

## 1.2 Attractor Neural Networks with Binary Units

One of the important problems in the study of memory processing is to recall the memory pattern as well as to store it. The models concerning these functions are called associative memory models or attractor neural networks. In the Hopfield model, we can achieve to store and recall patterns in the following way. We represent the state of the $j$-th unit at time $t$ as $S_j(t)$, where in this section, we assume that $S_j(t)$ takes 1 and $-1$ for mathematical

convenience. Then, the state of the $i$-th unit at time $t+1$ (if it is updated) is determined by

$$S_i(t+1) = \mathrm{sgn}\left(\sum_j J_{ij}S_j(t) - H_i\right), \tag{1.3}$$

where $\mathrm{sgn}(x)$ is defined by

$$\mathrm{sgn}(x) = \begin{cases} 1 & \text{for } x \geq 0 \\ -1 & \text{for } x < 0. \end{cases} \tag{1.4}$$

There are at least two updating rules, one is the synchronous updating rule and the other is the asynchronous updating rule. The former means that all units are updated simultaneously at each time step, on the other hand, the latter updates one unit at a time. In the Hopfield model, the asynchronous updating rule is adopted. We express the patterns to be embedded as $\xi_i^\mu$ $(i = 1, \cdots, N)$, where $\mu$ is the number of patterns and $N$ is the total number of units. Here we assume that $\xi_i^\mu$ takes 1 or $-1$ randomly. According to the Hebb's hypothesis, the patterns are embedded in the synaptic efficacies $J_{ij}$ taking the form,

$$\Delta J_{ij} \propto \xi_i^\mu \xi_j^\mu. \tag{1.5}$$

For the $P$ patterns to be stored, we adopt a following relation as synaptic connections

$$J_{ij} = \frac{1}{N}\sum_{\mu=1}^{P} \xi_i^\mu \xi_j^\mu. \tag{1.6}$$

Let us consider the case $P = 1$. When we set the pattern $\xi_i^1$ as the initial state of the system, that is, $S_i(0) = \xi_i^1$ for $i = 1, \cdots, N$, the next state of the site to be updated is determined by

$$S_i(1) = \mathrm{sgn}\left(\sum_j J_{ij}\xi_j^1\right). \tag{1.7}$$

Substituting $J_{ij} = \frac{1}{N}\xi_i^1\xi_j^1$ into Eq.(1.7) (Hereafter we assume $H_i = 0$.), we obtain

$$S_i(1) = \xi_i^1. \tag{1.8}$$

Consequently, the pattern $\xi_i^1$ is stable and can be considered to be stored in the system.



From the point of view of the memory processing, we have interests in the following problems.

- How many patterns can be stored and successfully retrieved?
- Can the system recover the original pattern $\xi_i^1$ from the noisy pattern $\xi_i^1$ + noise?

To answer these questions theoretically, we introduce several macroscopic order parameters and analyze them with the theory of statistical physics. The load parameter $\alpha$ is defined by $\frac{p}{N}$, which is called the storage capacity. To measure the similarity between the pattern $\xi_i^\mu$ and the state of the system at time $t$, we define the overlap by

$$m(t) = \frac{1}{N}\sum_{j=1}^{N} \xi_j^\mu S_j(t). \tag{1.9}$$

We note that $m(t)$ takes a value between $-1$ and 1. When the system has no correlations with a pattern, $m(t) = 0$. However, when the system has a correlation with a pattern, we should take care of treating $m(t)$. Let us consider the situations that $S_j(t) = \xi_j^\mu$ and $S_j(t) = -\xi_j^\mu$ for $j = 1, \cdots, N$. The overlap $m(t)$ takes 1 and $-1$ for the former and the latter case, respectively. However, from the point of view of information, there are no differences among them. Thus, it is appropriate to measure the similarity by the absolute value of $m(t)$. To answer the above questions corresponds to investigating the following properties.

- the maximum storage capacity

  As the embedded patterns are increased, the final overlap $m(\infty)$ becomes suddenly very small even when the initial state is set to the noiseless pattern. This critical storage capacity is called especially the maximum storage capacity and denoted by $\alpha_c$. It provides the answer of the former question.

- the basin of attraction

  Let us consider the situation that when we set the noisy pattern measured by $m_U(0)$

as the initial state, the final overlap $m(\infty)$ is near 1, however, when we set the noisy pattern measured by $m_L(0)$, the final overlap becomes almost zero. We may conjecture that there is a boundary between $m_L(0)$ and $m_U(0)$ that separates whether $m(\infty)$ becomes near 1 or almost 0. This boundary is called the basin of attraction and gives us the answer of the latter question.

- the critical overlap

  The final overlap $m(\infty)$ is needed to consider the above properties. It is called the critical overlap.

The associative process suggests the image of energy landscapes with valleys and hills on which the dynamical system relaxes toward one of the bottoms of the valleys illustrated in Fig.1.3 [6]. In this figure, each memory pattern corresponds to each bottom of the valleys, M1, M2 and M3. When the initial state of the system is enough similar to the pattern M2, the system retrieves the pattern M2 like a ball rolling down the valley. In this sense, the width of the valley is coordinate with the basin of attraction. As the number of embedded patterns is increased, the landscape becomes complicated and valleys whose bottoms are higher than those of memory patterns appear (see S1, S2 and S3 in Fig.1.3). They are also attractors where the system is trapped and referred to as spurious states. Considering these, the associative memory model is called the attractor neural network model. These analogies between the Hopfield model and physical systems enable us to apply the theory of statistical physics to the analysis of the associative memory model. For example, since the Hopfield model has the energy function

$$E\{S\} = -\frac{1}{2}\sum_{i\neq j} J_{ij}S_iS_j, \tag{1.10}$$

we can apply the replica method to calculate the maximum storage capacity, which is estimated by the investigation of the equilibrium state of the system [5]. To estimate



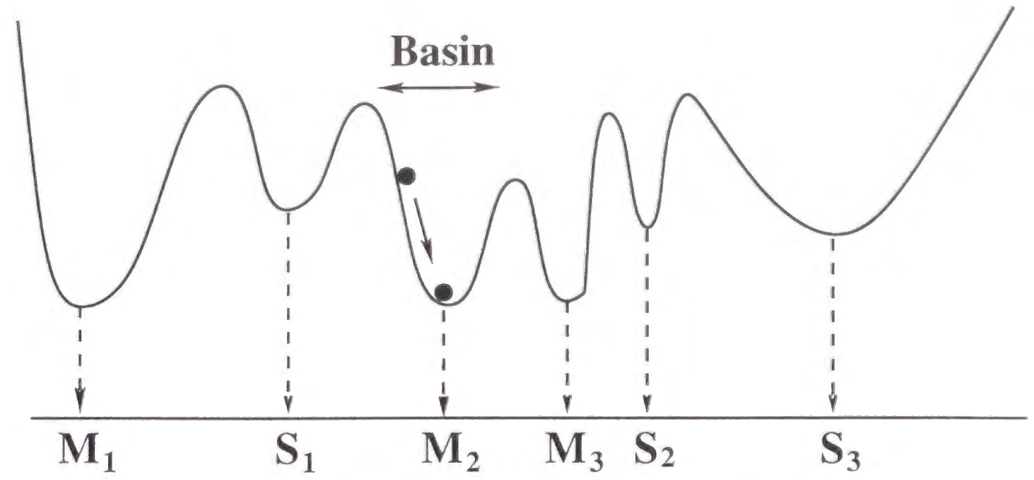


Figure 1.3: The one-dimensional landscape for associative memory.

the basin of attraction, it is necessary to study the retrieval process. This type of non-equilibrium state is difficult to treat, however, the theory of statistical neurodynamics proposed by Amari et al [7] and developed by Okada [9] enables us to investigate the synchronous updating model.

Although the patterns we treated above have no correlations among them since they are randomly generated, one of the important results was obtained in treating correlated patterns [10, 11, 12, 13, 14, 15]. Especially, Gardner found that the maximum storage capacity diverges proportionally to $1/a\ln a$ in the sparse coding limit $a \to 0$ [15] when the embedded patterns are defined by

$$\xi_i^\mu = \begin{cases} 1 & \text{with probability } a \\ -1 & \text{with probability } 1-a. \end{cases} \tag{1.11}$$

The coding condition such as $a \sim 0$ is called *sparse coding*. Since it is known that the level of activity in our brain is very low, it is very important to study the models concerning the above.

We can consider the attractor neural network as a module which provides a specific

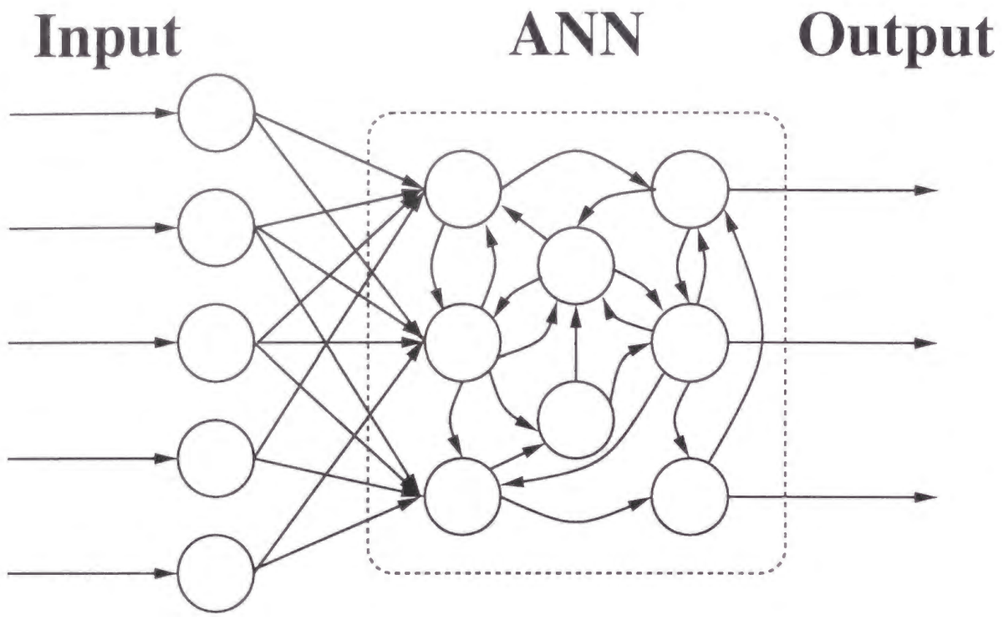


Figure 1.4: Depiction of input-output circuit with the attractor neural network

function. Let us consider the situation that we receive stimulus from the outer world and return a response. We can divide such a process of the nervous system into three parts, input, central processing and output. Furthermore, the central processing can be divided into neural systems with different functions and computational roles. Such neural systems receive the input, process it and transmit the output to the next module (see Fig.1.4). The function of each module should be a result of the interaction of large number of neurons, and thus, the attractor neural network appears in the system. We can say that the function is a result of learning, so it is considered as one kind of associative memories [6, 8].



## 1.3 Associative Memory Model with Oscillator Units

The Hopfield model is based on the assumption that information is coded only in the mean activity level of the neurons. In the model, the units takes only two states, firing and non-firing states. However, as the biological experiments make progress, it has been revealed that the dynamical aspects of neuronal activities such as synchronous oscillations of neuronal ensembles are computationally significant in information processing [16, 17, 18, 19, 20, 21]. Many authors have proposed models concerning these aspects [22, 23, 24]. It has been reported that under suitable conditions, models composed of oscillator units work as associative memory, and several properties such as maximum storage capacity and basin of attraction can be evaluated theoretically [25, 26, 27, 28, 29, 30, 31]. Cook showed that the maximum storage capacity of the oscillator model adopted a generalized Hebb rule with uncorrelated patterns is 0.038. Aoyagi et al showed the basin of attraction by analyzing the dynamics in the retrieval process. They suggested that the oscillator model is attractive one to treat the dynamical aspects of neurons because of the mathematical tractability as well as the associative ability.

## 1.4 Outline of the thesis

The oscillator models mentioned above are based on the unrealistic situation that all the components in the network are always in the firing state. Since we described previously that the activity of our brain is very low, it is necessary to consider temporal coding and sparse coding simultaneously.

In Chapter 2, we study the properties of oscillator neural networks treating sparsely coded phase patterns. In the former sections, we theoretically investigate basic properties such as maximum storage capacity and basin of attraction by applying the theory of statistical neurodynamics. Next, we consider several advanced features of our model. In

particular, we study the robustness against the synaptic dilution of the oscillator model and compare the results with those of the traditional Hopfield model.

In Chapter 3, we consider spurious states illustrated in Fig.1.3 of oscillator neural networks. The spurious state, which is also called mixed state, is formed as a result of storing patterns but not identical with them. Thus, we may consider that it is unnecessary and undesirable for information processing. However, as Miyashita showed that the formation of a concept pattern can be interpreted as a mixed state, it plays important roles in the memory processing [32]. In addition, several models concerning applications of mixed states to the information processing have been reported [33, 34]. For a mixed state on temporal coding models, Wang et al have reported the retrieval ability by numerical simulations [35], however, few theoretical studies have been presented. Therefore, we investigate theoretically the properties of mixed states. In the former sections in this chapter, we analyze the stability of the OR mixed state in an oscillator neural network. At last, we propose an interesting example of using mixed states in the information processing. We can say that introducing mixed states provides us an ability of solving the binding problem in a smart manner.

In the final chapter, we summarize the results and give some comments.

# Chapter 2

# Analysis of Oscillator Neural Networks for Sparsely Coded Phase Patterns

## 2.1 Introduction

One of the important but unsolved problems in neuroscience is to determine how information is coded in neuronal activities. Most of the traditional neural network models consisting of binary units are constructed on the assumption that information is coded only in the mean activity level of the neurons. Although these models have provided us with theoretically interesting information, they ignore many dynamical aspects of neuronal activities. In fact, oscillatory activity appears to be ubiquitous in many neuronal systems. For example, some recent biological experiments have revealed that spatially synchronous oscillations of neuronal ensembles are dependent on the global properties of the external stimulus. It has been suggested that such synchronization is computationally significant in information processing [16, 17, 18, 19, 20]. The hippocampus is also one of the areas in which neuronal synchronization is observed and is believed to play an important role in memory processing [20, 21] .

With these new findings, many models concerning the dynamical aspects of neurons and memory processing have been proposed [22, 23, 24]. Among these, models consisting



of networks of oscillator components are particularly attractive, owing to their mathematical tractability. Like the Hopfield model [3], the simplicity of these models allows us to obtain useful analytic results. In fact, it has been reported that under suitable conditions, the oscillator network models model associative memory, and we can theoretically evaluate their maximum storage capacities and basins of attraction [25, 26, 27, 28, 29, 30, 31].

However, such phase oscillator models are based on the unrealistic situation that all the components in the network are always in the firing state. In fact, real neurons can be in either the firing or non-firing state. In addition, it is known that the level of activity in our brain is very low. (i.e., at any given time only a small percentage of neurons are in the firing state.) This situation is termed *sparse coding*. From the results of theoretical studies of associative memory with binary units, it has been found that the storage capacity diverges as $-1/a \ln a$ as the activity level $a$ becomes small [10, 11, 12, 13, 14, 15].

It thus seems that to faithfully capture the essential dynamics of real oscillatory neuronal systems, it is necessary to extend the oscillator model to treat the non-firing state as well as the firing state.

In the next section, we first review the theoretical basis of the phase oscillator model and propose an extended version of the oscillator model to treat non-firing states. In the analysis of this model, we estimate the maximum storage capacity, derive the basin of attraction, and evaluate the quality of recalled memories. Then, we find that when we define the threshold as a dynamical variable in a certain manner, the size of the basin of attraction can be increased. Embedding patterns with different activity levels and the influence of synaptic dilution are also studied.

## 2.2 Basic Properties of Oscillator Neural Networks

### 2.2.1 Phase Oscillator Model

Let us first start with a survey of the theoretical basis of the phase oscillator model. We assume that neurons fire periodically and interact weakly with each other. In general, although such a neural system can be described in terms of many internal dynamical variables, it is well known that it can be reduced to a system of simple coupled phase oscillators [36, 37]. In this form, we can characterize the state of the $i$-th unit by a single variable, $\phi_i(t)$, which is referred to as the *phase*. This variable represents the timing of the neuronal spikes at time $t$. A typical reduced equation takes the form

$$\frac{d\phi_i(t)}{dt} = \omega_i(t) + \sum_{j=1}^{N} J_{ij} \sin(\phi_j(t) - \phi_i(t) + \beta_{ij}), \tag{2.1}$$

where $J_{ij}$ and $\beta_{ij}$ characterize the interaction between the $i$-th and $j$-th units. Assuming that all natural frequencies $\omega_i(t)$ are equal to some fixed value $\omega_0$, we can eliminate the $\omega_i(t)$ term in Eq.(2.1) by redefining $\phi_i(t)$ through $\phi_i(t) \to \phi_i(t) + \omega_0 t$. When we represent the state of the $i$-th unit by the complex form $W_i(t) = \exp(i\phi_i(t))$, Eq.(2.1) can be written in the alternative form

$$\frac{dW_i(t)}{dt} = \frac{1}{2}(h_i(t) - \tilde{h}_i(t)W_i^2(t)), \qquad h_i(t) = \sum_{j=1}^{N} C_{ij} W_j(t), \tag{2.2}$$

where the complex variable $C_{ij} = J_{ij}\exp(i\beta_{ij})$ represents the effect of the interaction between the $i$-th and $j$-th units and $\tilde{h}_i(t)$ is the complex conjugate of $h_i(t)$. (We assume $C_{ii} = 0$ throughout this paper.) Considering the fact that all units relax toward the equilibrium state satisfying the relation $W_i = h_i/|h_i|$, we can simplify the above to the discrete time system

$$W_i(t+1) = \frac{h_i(t)}{|h_i(t)|}, \quad h_i(t) = \sum_{j=1}^{N} C_{ij} W_j(t), \tag{2.3}$$

where the synchronous updating rule is assumed. We should remark that if we use *asynchronous* updating, the equilibrium states of Eq.(2.3) are equivalent to those of the original



phase model. This can be easily shown by considering the noiseless limit in a statistical mechanics treatment. In this sense, this model can be thought of as a synchronous update version of the phase oscillator neural network with discrete time [28].

### 2.2.2 Extended Model

The weakness of the model described by Eq.(2.3) is that it can only be used to treat the firing state. We wish to extend this model so that it has the ability of retrieving sparsely coded phase patterns. In Eq.(2.3), $h_i(t)$ can be regarded as the local field produced by all other units. This field determines the state of the i-th unit at the next time step. In a real neuron, when the membrane voltage is less than some threshold, the neuron generates no neuronal spikes. Therefore, it is reasonable to extend the above model so that the generation of spikes depends on the strength of the local field. Based on this consideration, for oscillator neural networks we propose the following generalized synchronous model [36, 37]:

$$W_i(t+1) = f(|h_i(t)|)\frac{h_i(t)}{|h_i(t)|}, \qquad h_i(t) = \sum_{j=1}^{N} C_{ij} W_j(t). \tag{2.4}$$

In this paper, we assume that $f(x) = \Theta(x - H)$, where $\Theta(x)$ is a step function defined by

$$\Theta(x) = \begin{cases} 1 & \text{for } x \geq 0 \\ 0 & \text{for } x < 0, \end{cases} \tag{2.5}$$

and $H$ is a threshold parameter controlling the activity of the network.

Figure2.1(a) displays the function $\Theta(x - H)$, and (b) illustrates the dynamical change at updating. Since the amplitude $|W_i(t+1)|$ depends on the threshold $H$, it has a strong influence on the activity of the system.

Now, we define a set of complex patterns denoted by $\xi_i^\mu = A_i^\mu \exp(i\theta_i^\mu)$ $(\mu = 1, \cdots, P$ ; $i = 1, \cdots, N)$, where $P$ is the total number of patterns and $N$ is the total number of units. The variables $\theta_i^\mu$ and $A_i^\mu$ represent the phase and the amplitude of the $i$-th unit

in the $\mu$-th pattern, respectively. For theoretical simplicity, we choose $A_i^\mu$ independently with the probability distribution:

$$A_i^\mu = \begin{cases} 1 & \text{for firing state with probability } a \\ 0 & \text{for silent state with probability } 1-a. \end{cases} \tag{2.6}$$

For the firing state, $\theta_i^\mu$ is chosen at random from a uniform distribution between 0 and $2\pi$. Note that all the patterns have the same mean activity level, $a$. As the learning rule, we adopt a generalized Hebb rule [4] taking the form

$$C_{ij} = \begin{cases} \frac{1}{aN}\sum_{\nu=1}^{P} \xi_i^\nu \tilde{\xi}_j^\nu & \text{for } i \neq j \\ 0 & \text{for } i = j. \end{cases} \tag{2.7}$$

Note that the matrix of the synaptic efficacies $C_{ij}$ is self-adjoint. This rule is based on the hypothesis that when the $i$-th and $j$-th neurons are firing simultaneously, the connection between them is enhanced, and otherwise no modification occurs [4]. We also note that this is slightly different from the covariance rule adopted in the context of the learning of sparsely coded patterns. Owing to the rotational symmetry of the phase distribution in the patterns, $C_{ij}$ can be defined in terms of the patterns $\xi_i^\nu$ themselves, rather than the difference between the patterns and the average activity.

We would like here to make some comments about this extended model. As mentioned above, it is well known that the dynamics of weakly coupled oscillatory neurons can be reduced to those of phase oscillators through a systematic theoretical technique. At the same time, this formalism can be also applied to a network of neuronal groups exhibiting periodic firing collectively, instead of a single neuron [37]. In this case, the phases of the oscillators can be regarded as the timings of the oscillatory behavior which such neuronal groups exhibit. Therefore, the phase is closely related to the timings of the neuronal spikes. In this paper, we have attempted to extend the previous model by introducing an amplitude variable phenomenologically in order to describe the non-firing state. By doing this, the relation between the model and real systems may become less apparent, but the dynamics of the phase variables are still able to model those of real systems.



Also, we believe that using a certain reduction technique, the relation between our model and real systems can be elucidated under suitable conditions. For example, we could consider a network consisting of neuronal systems exhibiting both oscillatory behavior and a non-firing state, and thus having both a limit cycle solution and a resting fixed point.

### 2.2.3 Theoretical Analysis

To analyze the recalling process theoretically, we must introduce several macroscopic order parameters. The load parameter $\alpha$ is defined by $\alpha = P/N$. The overlap $M^\mu(t)$ between $W_i(t)$ and $\xi_i^\mu$ at time $t$ is defined by

$$M^\mu(t) = m^\mu(t)\exp(i\varphi^\mu(t)) = \frac{1}{aN}\sum_{j=1}^{N} \tilde{\xi}_j^\mu W_j(t). \tag{2.8}$$

In practice, owing to rotational symmetry, the similarity between the state of the system $W_i(t)$ and the $\mu$-th pattern $\xi_i^\mu$ can be measured by $m^\mu(t)$, the amplitude of $M^\mu(t)$. Now, let us consider the situation in which the system is retrieving the pattern $\xi_i^1$, that is,

$$m(t) \equiv m^1(t) \sim O(1), \qquad m^\mu(t) \sim O\left(\frac{1}{\sqrt{N}}\right) \quad (\mu \neq 1). \tag{2.9}$$

The local field $h_i(t)$ can be separated as

$$h_i(t) = M^1(t)\xi_i^1 + z_i(t) = |\xi_i^1| m(t) e^{i(\varphi^1(t)+\theta_i^1)} + z_i(t), \tag{2.10}$$

where $z_i(t)$ is defined by

$$z_i(t) = \frac{1}{aN}\sum_{j,\nu\neq 1} \xi_i^\nu \tilde{\xi}_j^\nu W_j(t). \tag{2.11}$$

The first term in Eq.(2.10) is the signal driving the system to recall the pattern, and the second term can be regarded as the noise arising from the other learned patterns. It is the essence of our analysis that we treat the second noise term as a complex Gaussian noise characterized by

$$< z_i(t) >_i = 0, \quad < |z_i(t)|^2 >_i = 2\sigma^2(t). \tag{2.12}$$

It has been confirmed with numerical simulations that the assumption is valid as long as the network succeeds in retrieval [38]. Under the above assumptions, we study the properties of this network by applying the methods of statistical neurodynamics [7, 39, 9, 40]. To begin with, we calculate the overlap at time $t+1$. From Eqs.(2.8), (2.4) and (2.10), $M^1(t+1)$ is given by

$$\begin{aligned} M^1(t+1) &= m(t+1)\exp(i\varphi^1(t+1)) = \frac{1}{aN}\sum_{j=1}^{N}\tilde{\xi}_j^1 f(|h_j(t)|)\frac{h_j(t)}{|h_j(t)|} \\ &= \frac{1}{aN}\sum_j \tilde{\xi}_j^1 f(|\xi_j^1 M^1(t)+z_j(t)|)\frac{\xi_j^1 M^1(t)+z_j(t)}{|\xi_j^1 M^1(t)+z_j(t)|}. \end{aligned}$$

Now, we assume that the phase of $M^1(t+1)$ is almost constant, that is, $\varphi^1(t+1)\approx\varphi_0$. The validity of this assumption is supported by the results of preliminary numerical simulations. Owing to the rotational symmetry of the complex Gaussian noise, we can replace $z_j(t)$ with $z_j(t)\exp[i(\varphi_0+\theta_j^1)]$. After some calculations, in the limit $N\to\infty$, we obtain

$$\begin{aligned} m(t+1) &= \frac{1}{aN}\sum_j |\xi_j^1| f(||\xi_j^1|m(t)+z_j(t)|)\frac{|\xi_j^1|m(t)+z_j(t)}{||\xi_j^1|m(t)+z_j(t)|} \\ &= \left\langle\left\langle f(|m(t)+z(t)|)\frac{m(t)+z(t)}{|m(t)+z(t)|}\right\rangle\right\rangle_{z(t)}, \end{aligned} \tag{2.13}$$

where $\ll \quad \gg_{z(t)}$ represents the average over the complex Gaussian noise $z(t)$ defined by Eq.(2.12). To calculate Eq.(2.13) numerically, we need the value of $\sigma(t)$, which is the variance of $z(t)$. Thus, in the next step, we consider the relation between $z_i(t+1)$ and $z_i(t)$, from which we can obtain the relation between $\sigma(t+1)$ and $\sigma(t)$. From Eq.(2.11), the noise at time $t+1$ can be written as

$$\begin{aligned} z_i(t+1) &= \frac{1}{aN}\sum_{j,\nu\neq 1}\xi_i^\nu\tilde{\xi}_j^\nu W_j(t+1) \\ &= \frac{1}{aN}\sum_{j,\nu\neq 1}\xi_i^\nu\tilde{\xi}_j^\nu f(|h_j(t)|)\frac{h_j(t)}{|h_j(t)|} \\ &= \frac{1}{aN}\sum_{j,\nu\neq 1}\xi_i^\nu\tilde{\xi}_j^\nu f(|h_j^{-\nu}(t)+h_j^\nu(t)|)\frac{h_j^{-\nu}(t)+h_j^\nu(t)}{|h_j^{-\nu}(t)+h_j^\nu(t)|}, \end{aligned} \tag{2.14}$$



where $h_j^{-\nu}(t)$ and $h_j^\nu(t)$ are defined by

$$h_j^{-\nu}(t) = \frac{1}{aN}\sum_{k,\mu\neq\nu}\xi_j^\mu\tilde{\xi}_k^\mu W_k(t), \quad h_j^\nu(t) = \frac{1}{aN}\sum_k \xi_j^\nu\tilde{\xi}_k^\nu W_k(t). \tag{2.15}$$

Note that these functions satisfy the relation $h_j(t) = h_j^{-\nu}(t)+h_j^\nu(t)$. We can carry out the summation in Eq.(2.14) under the assumption that $h_j^{-\nu}(t)$ is independent of $\xi_i^\nu$. Doing so, we obtain

$$z_i(t+1) \simeq K(m(t),\sigma(t)) + z_i(t)G(m(t),\sigma(t)) \tag{2.16}$$

$$K(m(t),\sigma(t)) = \frac{1}{aN}\sum_{j,\nu\neq 1}\xi_i^\nu\tilde{\xi}_j^\nu f(|h_j(t)|)\frac{h_j(t)}{|h_j(t)|} \tag{2.17}$$

$$\begin{aligned} G(m(t),\sigma(t)) = \Bigg\langle\Bigg\langle a\left(\frac{f'(|m(t)+z(t)|)}{2}+\frac{f(|m(t)+z(t)|)}{2|m(t)+z(t)|}\right) \\ +(1-a)\left(\frac{f'(|z(t)|)}{2}+\frac{f(|z(t)|)}{2|z(t)|}\right)\Bigg\rangle\Bigg\rangle_{z(t)}, \end{aligned} \tag{2.18}$$

where $f'$ means the derivative of $f$.

Note that Eqs.(2.16), (2.17) and (2.18) are needed to calculate $\sigma$ in both the equilibrium and the non-equilibrium cases we will describe in the next two sections.

### 2.2.4 Equilibrium State

In this section, we consider the equilibrium state of our model, in which $z_i(t)$ is constant. Applying $z_i(t+1) = z_i(t) = z_i$ to Eq.(2.16), we obtain

$$z_i = \frac{K}{1-G}. \tag{2.19}$$

Using this equation, we immediately obtain

$$2\sigma^2 = <|z_i|^2>_i = \frac{|K|^2}{(1-G)^2}, \tag{2.20}$$

where

$$|K|^2 = \alpha\left\langle\left\langle af(|m+z|)+(1-a)f(|z|)\right\rangle\right\rangle_z \tag{2.21}$$

$$\equiv \alpha Q. \tag{2.22}$$

Consequently, we find that the equilibrium state satisfies the equations

$$m = \left\langle\left\langle f(|m+z|)\frac{m+z}{|m+z|}\right\rangle\right\rangle_z \tag{2.23}$$

$$\sigma^2 = \frac{\alpha}{2(1-G)^2}Q \tag{2.24}$$

$$G = \left\langle\left\langle a\left(\frac{f'(|m+z|)}{2}+\frac{f(|m+z|)}{2|m+z|}\right)+(1-a)\left(\frac{f'(|z|)}{2}+\frac{f(|z|)}{2|z|}\right)\right\rangle\right\rangle_z \tag{2.25}$$

$$Q = \langle\langle af(|m+z|)+(1-a)f(|z|)\rangle\rangle_z . \tag{2.26}$$

Solving the above equilibrium equations, we can find two types of solutions. If the load parameter $\alpha$ is smaller than a certain value $\alpha_c$, there exists a solution for which the overlap $m$ between the system and the pattern is not zero. As $m \neq 0$ implies that the system has a correlation with the retrieved pattern, this solution corresponds to the retrieval state. Then, if $\alpha$ is larger than $\alpha_c$, there is only one solution, and for this solution $m = 0$. This solution therefore corresponds to the non-retrieval state.

The critical load parameter $\alpha_c$ is called "the maximum storage capacity". We now examine our theoretical results by comparing them with results from numerical simulations. In Fig.2.2(a), we show the dependence of $\alpha_c$ on several parameters, such as the threshold $H = 0.3, 0.5, 0.8$ and the activity level $a$. In (a), We can see that as the activity level $a$ decreases, the storage capacity $\alpha_c$ increases for each $H$. In particular, in the limit $a \to 0$, we numerically find that the storage capacity diverges in proportion to $-1/a \ln a$, as in the case of the Hopfield model. The maximum storage capacity as a function of $a$ and $H$ is illustrated in (b). It is shown there that for any $H$, the storage capacity diverges as $a$ decreases to zero.



### 2.2.5 Non-equilibrium State

In this section, we derive dynamical equations to study the retrieving process. To obtain a recursion equation for $\sigma$, we start with Eq.(2.16). Squaring Eq.(2.16), we obtain

$$2\sigma^2(t+1) = \alpha Q(m(t),\sigma(t)) + 2\sigma^2(t)G^2(m(t),\sigma(t)) + 2Re\left\langle\left\langle K(m(t),\sigma(t))\tilde{z}_i(t)\tilde{G}(m(t),\sigma(t))\right\rangle\right\rangle_{z(t)}, \tag{2.27}$$

where $K(m(t),\sigma(t))$ and $G(m(t),\sigma(t))$ are given by Eqs.(2.17) and (2.18), and

$$Q(m(t),\sigma(t)) = \langle\langle\ af(|m(t)+z(t)|)+(1-a)f(|z(t)|)\ \rangle\rangle_{z(t)} . \tag{2.28}$$

To proceed with the calculation, we must estimate the time correlation of the noise. For the first-order approximation, we ignore the temporal correlation of $z_i(t)$. We then obtain

$$\sigma^2(t+1) = \frac{\alpha}{2}Q(m(t),\sigma(t)) + \sigma^2(t)G^2(m(t),\sigma(t)) + \alpha a^2 m(t+1)m(t)G(m(t),\sigma(t)). \tag{2.29}$$

This corresponds to the Amari-Maginu theory in the case of traditional neural networks [7].

For the second-order approximation, we take into account the fact that $z_i(t)$ is correlated only with $z_i(t-1)$, while all correlations with $z_i(t')$ for $t' < t-1$ are ignored. In this case, $\sigma(t+1)$ can be obtained from

$$\sigma^2(t+1) = \frac{\alpha}{2}Q(m(t),\sigma(t)) + \sigma^2(t)G^2(m(t),\sigma(t)) + \alpha G(m(t),\sigma(t))X(t+1,t) + \alpha a^2 m(t+1)m(t-1)G(m(t),\sigma(t))G(m(t-1),\sigma(t-1)), \tag{2.30}$$

where $Q(m(t),\sigma(t))$ is given by Eq.(2.28), $G(m(t),\sigma(t))$ is given by Eq.(2.18), and

$$X(t+1,t) = Re < W_j(t+1)\tilde{W}_j(t) >_j . \tag{2.31}$$

Here,

$$\rho(t,t-1) = \frac{\alpha X(t,t-1)}{2\sigma(t)\sigma(t-1)} + \frac{\sigma(t-1)}{\sigma(t)} G(m(t-1),\sigma(t-1)) \tag{2.32}$$

is needed to evaluate Eq.(2.31). Note that $\rho(t,t-1)$ is the correlation coefficient between $z(t)$ and $z(t-1)$. For the second order approximation, consequently, the retrieving process of the network is described by the equations

$$\begin{aligned} m(t+1) &= \frac{1}{aN}\sum_j |\xi_j^1| f(||\xi_j^1| m(t) + z_j(t)|) \frac{|\xi_j^1| m(t) + z_j(t)}{||\xi_j^1| m(t) + z_j(t)|} \\ &= \left\langle\left\langle f(|m(t)+z(t)|)\frac{m(t)+z(t)}{|m(t)+z(t)|}\right\rangle\right\rangle_{z(t)} \qquad (2.33) \\ \sigma^2(t+1) &= \frac{\alpha}{2} Q(m(t),\sigma(t)) + \sigma^2(t) G^2(m(t),\sigma(t)) \\ &\quad + \alpha G(m(t),\sigma(t)) X(t+1,t) \qquad (2.34) \\ &\quad + \alpha a^2 m(t+1) m(t-1) G(m(t),\sigma(t)) G(m(t-1),\sigma(t-1)) \\ X(t+1,t) &= Re < W_j(t+1)\tilde{W}_j(t) >_j \qquad (2.35) \\ \rho(t,t-1) &= \frac{\alpha X(t,t-1)}{2\sigma(t)\sigma(t-1)} + \frac{\sigma(t-1)}{\sigma(t)} G(m(t-1),\sigma(t-1)) \qquad (2.36) \\ G(m(t),\sigma(t)) &= \left\langle\left\langle a\left(\frac{f'(|m(t)+z(t)|)}{2} + \frac{f(|m(t)+z(t)|)}{2|m(t)+z(t)|}\right)\right.\right. \qquad (2.37) \\ &\quad \left.\left. + (1-a)\left(\frac{f'(|z(t)|)}{2} + \frac{f(|z(t)|)}{2|z(t)|}\right)\right\rangle\right\rangle_{z(t)} \\ Q(m(t),\sigma(t)) &= \langle\langle\ a f(|m(t)+z(t)|) + (1-a) f(|z(t)|)\ \rangle\rangle_{z(t)}\,. \qquad (2.38) \end{aligned}$$

For initial conditions, we choose $\sigma^2(0) = a\alpha/2$, $X(0,-1) = 0$ and $X(1,0) = a^2 m(1) m(0)$. We choose many values of the initial overlap $m(0)$ and carry out numerical calculations for each. In this way, we determine the lower bound, under which the network fails to retrieve the pattern.

For higher-order approximations, we could derive similar generalized equations describing the retrieval dynamical process. However, as shown in Fig.2.3, the theoretical prediction at second order gives reasonable agreement with the numerical simulation in contrast to that at first order. We thus conclude that it is sufficient to use the second-order



approximation for the theoretical analysis in this paper.

Figure2.4 displays a phase diagram for $m(0)_c$ and $m(\infty)$ at various mean activity levels $a$ and thresholds $H$. The solid lines and the data points here correspond to the theoretical and the numerical results, respectively. It is seen that even in the region satisfying $\alpha < \alpha_c$, the system cannot retrieve the pattern if the initial overlap $m(0)$ is smaller than $m(0)_c$. The boundary corresponding to $m(0)_c$ is represented by the lower curves in Fig.2.4. Thus, for $m(0) \geq m(0)_c$, $m(t)$ reaches the value of the upper curves $m(\infty)$, while for $m(0) < m(0)_c$, $m(t)$ decreases to zero. We should note that the basins of attraction remain wide even near $\alpha_c$. This can be thought of as an advantage of associative memory.

To predict the correct behavior of the retrieval dynamics, it is necessary for the time correlation of the noise terms to be taken into account, and thus the second-order approximation discussed above is necessary. In the case we consider, this order is also sufficient, but interestingly, it has been reported that the fourth-order approximation is necessary when $a = 1$ and $H = 0$ [28]. The question arises why the second-order approximation is not sufficient in this case, while it is sufficient in the case we consider. The key point here is that the order of the last term in Eq.(2.34) is proportional to the square of the activity level $a^2$. For $a < 1$, this factor $a^2$ weakens the influence of the time correlation on the recalling process. Consequently, for a sparse coded pattern with $a < 1$, even the second-order approximation results in reasonable agreement with the numerical results.

## 2.3 Advanced Properties of Oscillator Neural Networks

### 2.3.1 Sequence Generator

In this section, we consider the case in which the network retrieves a cyclic sequence of $P$ patterns associatively, say $\xi^1 \to \xi^2 \to \cdots \to \xi^P \to \xi^1 \to \cdots$. In order to allow for such

a process, we employ synaptic connections of the form

$$C_{ij} = \frac{1}{aN} \sum_{\nu=1}^{P} \xi_i^{\nu+1} \tilde{\xi}_j^{\nu}. \tag{2.39}$$

In a manner similar to that in the derivation of Eqs.(2.29) and (2.34), we obtain the following equations:

$$\sigma^2(t+1) = \frac{\alpha}{2} Q(m(t), \sigma(t)) + \sigma^2(t) G^2(m(t), \sigma(t)) \tag{2.40}$$

$$m(t+1) = \left\langle \left\langle f(|m(t)+z(t)|) \frac{m(t)+z(t)}{|m(t)+z(t)|} \right\rangle \right\rangle_{z(t)}. \tag{2.41}$$

Note that, since the target pattern changes from time to time, for the definition of the overlap we adopt $m(t) \equiv m^{\mu}(t) = |\frac{1}{aN} \sum_{j=1}^{N} \tilde{\xi}_j^{\mu} W_j(t)|$, where $\mu$ is the number of the target pattern at time $t$. Here $G(m(t), \sigma(t))$ and $Q(m(t), \sigma(t))$ are the same as those defined by Eqs.(2.37) and (2.38), respectively. We should note that in the limit $N \to \infty$, the last term in Eqs.(2.29) and (2.34) vanishes in Eq.(2.40), because the effect of the time correlation can be ignored in the above derivation. Therefore, in a sequence generator, it is expected that our theoretical prediction is almost exact.

Figure2.5(a) displays a phase diagram obtained from our theoretical analysis. All the lines of theoretical results agree with the numerical ones quite well, as expected. This agreement suggests that higher-order approximations will result in even better agreement and leads us to believe that our theoretical derivation is valid. In (b), it is also shown that, like auto-associative memory (Fig.2.2(b)), the storage capacity diverges in the limit $a \to 0$. This is regarded as expressing the meaning that in the limit of sparse coding (i.e., as $a \to 0$), we can embed an infinite length of sequential patterns.

### 2.3.2 Dynamically Adjusted Threshold

From Fig.2.4, it appears that the basin of attraction for our model is smaller than those in the binary model and the phase oscillator. In this section, we attempt to increase



the size of the basin of attraction by defining the threshold as a dynamical variable that is proportional to the standard deviation of the noise. Therefore, assuming the same condition as in Sec.2.2.2, we add the equation

$$H(t) = \sqrt{-2 \ln a} \sigma(t), \tag{2.42}$$

where $H(t)$ is the threshold at time $t$. This choice for the form of $H(t)$ is made to insure the relations $m \simeq 1$ and [activity level] $\simeq a$, which cause the Hamming distance between the state of the unit and the retrieved pattern to be small [41]. Comparing Fig.2.6 with Fig.2.4, it is seen that the basin of attraction can be enlarged by introducing the dynamically adjusted threshold into our model. Therefore, when we introduce the dynamically adjusted threshold, our model has an advantage similar to that of the binary model and the phase oscillator.

### 2.3.3 Patterns Generated with Different Activity Levels

To this point, we have assumed that the activity levels are equal for all patterns. However, it is likely that the actual activity level depends on the pattern which the network is retrieving presently, in other words, on the content of the required information processing. Unfortunately, using a traditional neural network, we encounter difficulties in storing patterns with different activity levels simultaneously. In this section, we demonstrate that, unlike traditional models, the proposed oscillator model can easily store multiple patterns with different activity levels using a simple Hebbian learning rule.

Let us consider a set of complex patterns defined by

$$Prob[|\xi_i^{\mu}| = 1] = \begin{cases} a_1 & \text{for } 1 \le \mu \le P_1 \\ a_2 & \text{for } P_1 + 1 \le \mu \le P, \end{cases} \tag{2.43}$$

where generally $a_1 \neq a_2$. Thus, the total number of the patterns with activity level $a_1$ is $P_1$, while the total number of patterns with the activity level $a_2$ is $P_2 = P - P_1$. Using the above patterns, grouped into two different activity levels, we examine whether the

network can retrieve patterns having different activity levels. To retrieve such patterns, we use the following modified form of the learning rule Eq.(2.7):

$$C_{ij} = \frac{1}{a_1 N} \sum_{\nu=1}^{P_1} \xi_i^\nu \tilde{\xi}_j^\nu + \frac{1}{a_2 N} \sum_{\nu=P_1+1}^{P} \xi_i^\nu \tilde{\xi}_j^\nu. \tag{2.44}$$

With the method described in Sec.2.2, we can derive both equilibrium and dynamical equations. The results have the same forms as those in Sec.2.2. However, here the value $a_1$ should be used in place of the activity parameter $a$ in the previous equations, because the retrieval pattern $\xi_i^1$ has an activity level $a_1$. Let us define the load parameter as $\alpha_1 = P_1/N$ with respect to the retrieval pattern. (The usual load parameter is defined as $\alpha = P/N = (P_1 + P_2)/N$.) The theoretical analysis yields $\alpha_{1c} = const. - \alpha_2$, where $\alpha_{1c}$ is the maximum storage capacity for $a_1$, and $\alpha_2$ is the storage capacity for $a_2$. Figure2.7 displays $\alpha_{1c}$ as a function of $\alpha_2 = P_2/N$. We can see from Fig.2.7 that $\alpha_{1c} = \alpha(a_1) - \alpha_2$, where the constant value $\alpha(a_1)$ is given by the equations in (2.23), (2.24), (2.25) and (2.26) for $a = a_1$. For the maximum storage capacity $\alpha_{2c}$ associated with the activity level $a_2$, we have $\alpha_{2c} = \alpha(a_2) - \alpha_1$.

Let us consider the case $P_1 = P_2$. Note that in this case, $\alpha_1 = \alpha_2$ and the total storage capacity $\alpha$ has the relation as $\alpha = 2\alpha_1 = 2\alpha_2$. We assume that $a_1 = 0.1$, $a_2 = 0.2$ and $H = 0.3$. Under these conditions, the basin of attraction obtained both from the theoretical analysis and the numerical simulations is displayed in the left panel of Fig.2.8. We should note that in the region (b), the patterns with activity $a_1$ can be recalled, while the patterns with activity $a_2$ cannot. Since we consider the case $P_1 = P_2$, the vertical lines correspond to half of the usual maximum storage capacities. In the right figures, we display typical behavior of the overlap $m(t)$ for the initial condition $m(0) = 0.5$. The load parameters $\alpha = 0.02, 0.05$ and $0.08$ used here correspond to the regions (a), (b) and (c) shown in the left figure, respectively. The evolutions corresponding to these values of $a$ represent the retrieval processes of $\xi_i^1$ and $\xi_i^{P_1+1}$ associated with the activity levels $a_1$ and



$a_2$, respectively. Note that in the region (b), the patterns with $a = 0.2$ act only as noise when the network is recalling the pattern with $a = 0.1$. As a whole, the above findings suggest that the network has a good ability to retrieve patterns with different activity levels. We should remark that the patterns with activity $a_1$ can be stored more stably rather than those with activity $a_2$ when $a_1 < a_2$.

### 2.3.4 Dilution

In this section, we study the influence of random synaptic dilution on the model's associative memory capability. For the case of the phase oscillator model, that is, when $a = 1$ and $H = 0$, this effect has already been reported [31, 29]. Following the method used in that case to treat random synaptic dilution in our model, we assume that the synaptic efficacies for $j \neq i$ take the form

$$\overline{C}_{ij} = \frac{c_{ij}}{c} C_{ij}, \tag{2.45}$$

where $C_{ij}$ is the standard Hebbian matrix, as defined by Eq.(2.7), and, the $c_{ij}$ are independent random variables, taking the values 1 and 0 with probabilities $c$ and $1-c$, respectively. Note that the dilution parameter $c$ represents the ratio of connected synapses. In the limit $N \to \infty$, Eq.(2.45) can be regarded as

$$\overline{C}_{ij} = C_{ij} + \eta_{ij}, \tag{2.46}$$

where the synaptic noise $\eta_{ij}$ is a complex Gaussian noise with mean 0 and variance $\eta^2/N$ [42]. The relationship between the dilution parameter $c$ and the variance $\eta$ can be calculated as

$$\eta^2 = \frac{1-c}{c}\alpha. \tag{2.47}$$

Under the same assumption as that used in obtaining Eq.(2.9), we can separate the local field into the signal and two noise parts as follows:

$$\begin{aligned} h_i(t) &= \sum_j^N \overline{C}_{ij} W_j(t) \\ &= \sum_j^N (C_{ij} + \eta_{ij}) W_j(t) \\ &= \sum_j^N (\frac{1}{aN} \sum_{\mu=1}^P \xi_i^\mu \tilde{\xi_j^\mu} + \eta_{ij}) W_j(t) \\ &= M^1(t)\xi_i^1 + z_i(t) \qquad (2.48) \\ &= M^1(t)\xi_i^1 + z_i^c(t) + z_i^s(t), \qquad (2.49) \end{aligned}$$

where $z_i^c(t)$ and $z_i^s(t)$ are defined as

$$\begin{aligned} z_i^c(t) &= \frac{1}{aN} \sum_j^N \sum_{\mu \neq 1}^P \xi_i^\mu \tilde{\xi_j^\mu} W_j(t) \qquad (2.50) \\ z_i^s(t) &= \sum_j^N \eta_{ij} W_j(t). \qquad (2.51) \end{aligned}$$

The new noise term $z_i^s(t)$ is caused by synaptic dilution, while the term $z_i^c(t)$ is like the noise defined by Eq.(2.11), representing the crosstalk noise arising from the other embedded patterns. In analogy to our treatment in Sec.2.2, we assume that $z_i^c(t)$ and $z_i^s(t)$ are independent complex Gaussian noises with mean 0 and variance $\sigma_c^2(t)$ and $\sigma_s^2(t)$, respectively. Therefore, $z_i(t)$ can be regarded as a complex Gaussian noise with mean 0 and variance $2\sigma^2(t) = \sigma_c^2(t) + \sigma_s^2(t)$. Thus, we can derive dynamical equations in the same way as in Sec.2.2. The form of the macroscopic order parameter $m(t+1)$ is the same as that given by Eq.(2.13).

First, applying the theory of statistical neurodynamics to $z_i^s(t)$, we calculate $\sigma_s^2(t)$. However, to apply the theory of statistical neurodynamics, it is necessary to take into account the second term in

$$z_i^s(t+1) = \sum_j^N \eta_{ij} f(|h_j^0|) \frac{h_j^0}{|h_j^0|} + W_i(t) \sum_j^N \eta_{ij}\eta_{ji} \left( \frac{f'(|h_j^0|)}{2} + \frac{f(|h_j^0|)}{2|h_j^0|} \right), \qquad (2.52)$$



where $h_j^0 = h_j(t) - \eta_{ji} W_i(t)$. As reported in [29], for the asymmetrical case, $\eta_{ij} \neq \eta_{ji}$, the second term here can be ignored. Then, as seen from Fig.(2.9), there is little difference between symmetric and asymmetric cases in a sparse coding system. Thus we conjecture that this term can be ignored altogether. Doing so, in the $N \to \infty$ limit, we obtain

$$\begin{aligned} \sigma_s^2(t) &= \eta^2 Q(m(t), \sigma(t)) \\ &= \frac{1-c}{c} \alpha Q(m(t), \sigma(t)), \qquad (2.53) \end{aligned}$$

where $Q(m(t), \sigma(t))$ is defined by Eq.(2.38).

For the crosstalk noise $z_i^c(t)$, in analogy to Eq.(2.16), we obtain

$$z_i^c(t+1) = K(m(t), \sigma(t)) + z_i^c(t) G(m(t), \sigma(t)), \qquad (2.54)$$

where $K(m(t), \sigma(t))$ and $G(m(t), \sigma(t))$ are defined by Eqs.(2.17) and (2.18), respectively.

### 2.3.5 Equilibrium State

In the equilibrium state, putting $z_i^c(t) = z_i^c(t+1)$ into Eq.(2.54), we obtain

$$\begin{aligned} z_i^c &= \frac{K}{1-G} \qquad (2.55) \\ \sigma_c^2 &= \frac{\alpha Q}{(1-G)^2}. \qquad (2.56) \end{aligned}$$

Therefore, $\sigma^2$, the variance of $z(t)$, takes the form

$$\begin{aligned} \sigma^2 &= \frac{1}{2}\sigma_c^2 + \frac{1}{2}\sigma_s^2 \\ &= \left( \frac{1}{2(1-G)^2} + \frac{1-c}{2c} \right) \alpha Q. \qquad (2.57) \end{aligned}$$

Consequently, the properties of the network in the equilibrium state can be calculated from Eqs.(2.23), (2.57), (2.25) and (2.26). In Fig.2.10, we summarize the theoretical results concerning the dependence on the ratio of connected synapses $c$. In Fig.2.10(a), it is found that the maximum storage capacity is an increasing function of the connectivity

$c$. Particularly, we can see that, as the activity level $a$ becomes small, the storage capacity decreases almost linearly with the connectivity $c$. A similar linear dependence is observed in the case of the diluted Hopfield model. On the other hand, in (b), it is found that even if the ratio of connectivity is small, the maximum storage capacity tends to diverge in the limit $a \to 0$. However, it seems that the rate of this divergence decreases as $c$ decreases.

### 2.3.6 Non-equilibrium State

In order to estimate the robustness with respect to synaptic damage, we should also consider the influence of synaptic dilution on the retrieval process, particularly, on the basin of attraction. For this purpose, we can apply the same method as used in the derivation of Eq.(2.34). After some calculations, the resulting recursion equations at second order are given by

$$\begin{aligned}
\sigma^2(t+1) &= \frac{\alpha}{2}Q(m(t),\sigma(t)) + \sigma^2(t)G^2(m(t),\sigma(t)) \\
&\quad +\alpha G(m(t),\sigma(t))X(t+1,t) \\
&\quad +\alpha a^2 m(t+1)m(t-1)G(m(t),\sigma(t))G(m(t-1),\sigma(t-1)) \\
&\quad +\frac{1}{2}(1-G^2(m(t),\sigma(t)))\eta^2 Q(m(t),\sigma(t)) \qquad (2.58) \\
X(t+1,t) &= Re < W_j(t+1)\tilde{W}_j(t) >_j \qquad (2.59) \\
\rho(t,t-1) &= \frac{\alpha X(t,t-1)}{2\sigma(t)\sigma(t-1)} + \frac{\sigma(t-1)}{\sigma(t)}G(m(t-1),\sigma(t-1)) \qquad (2.60) \\
&\quad +\frac{X(t,t-1) - G(m(t-1),\sigma(t-1))Q(m(t-1),\sigma(t-1))}{2\sigma(t)\sigma(t-1)}\eta^2,
\end{aligned}$$

where $\eta$ is related to the connectivity $c$ via Eq.(2.47). As mentioned in Sec.2.2, Eq.(2.60) is used to calculate Eq.(2.59). For initial conditions, we choose $\sigma^2(0) = a\alpha/2c$, $X(0,-1) = 0$ and $X(1,0) = a^2 m(1)m(0)$. In the case of $a = 0.1$ and $H = 0.5$, Fig.2.11 illustrates the theoretical results concerning the basins of attraction for various values of the connectivity $c$. We can see that near saturation $\alpha \sim \alpha_c$, the basin of attraction remains large even for low connectivity. Therefore, we find that synaptic dilution has little influence on the



width of the basin of attraction, even though the storage capacity decreases with the connectivity.

## 2.4 Conclusion

In this chapter, we have presented a simple extended model of oscillator neural networks to allow for the description of the non-firing state. We have studied the model's associative memory capability for sparsely coded phase patterns, in which some units are in the non-firing state and the other units encode information in the phase variable representing the timing of neuronal spikes. In particular, applying the theory of statistical neurodynamics, we have evaluated the maximum storage capacity and derived the basin of attraction. We have found the following properties of our model in its basic form:

- In both case of auto-associative memory and sequence generators, the storage capacity diverges as the activity level decreases to zero. It was numerically found that the storage capacity diverges proportionally with $-1/a \ln a$ in the limit $a \to 0$.
- Even just below the maximum storage capacity, the basin of attraction remains large.

We then investigated the model with regard to the size of the basin of attraction. We found that with the model in its basic form, the basin of attraction is smaller than those of the binary model and the phase oscillator. For associative memory, it is desirable that the basin of attraction be large. For this reason, we considered employing a dynamically adjusted threshold, and we found the following:

- The basin of attraction can be enlarged by using the dynamically adjusted threshold.

In view of biology, the neurons may die of age or be injured by accident. Thus, the robustness with respect to synaptic damage is important for real neuronal systems. For

this reason, we also investigated our model with regard to robustness, and we found the following:

- It was found that the system is robust with respect to synaptic damage: Even in the case of a high cutting rate, the basin of attraction remains large, and the maximum of the storage capacity diverges in the $a \to 0$ limit. For low activity patterns, the maximum storage capacity decreases almost linearly with the ratio of connected synapse.

The above properties are common with the Hopfield model. In addition, we have found that our model possesses a novel feature not seen in the Hopfield model. In realistic situations, the activity level of the firing pattern may generally depend on the content of the information processing. Using traditional neural network models based only on activity rate coding, however, we encounter difficulties when the network simultaneously stores such patterns with different activity levels. Contrastingly, with our model, we found the following:

- Unlike the Hopfield model, provided that the phase distribution in the embedded patterns is uniform, it was shown that patterns with different activity levels can be memorized simultaneously.

In conclusion, from the above findings it is seen that the oscillator neural network exhibits good performance in the case of sparse coding. In this situation, the phases of the oscillators can be regarded as the timings of oscillations in the original system, which are closely related to the timings of the neuronal spikes. This implies that in our model information is encoded by the relative timing of oscillations, which corresponds to spikes in the original system. This is one type of temporal coding. In this sense, we believe that these results support the plausibility of temporal coding.



In the description provided by our model, a firing state and a non-firing state correspond to the existence of a limit cycle solution and a steady solution, respectively, even if a very low frequency is considered. However, to obtain interesting results, we have assumed that the native frequencies of all neurons are the same. This may be biologically unrealistic. In addition, we have not considered the probabilistic nature of the synapses and neurons, which may play an important role in the information processing. A more realistic treatment in which these points are considered more carefully is needed.

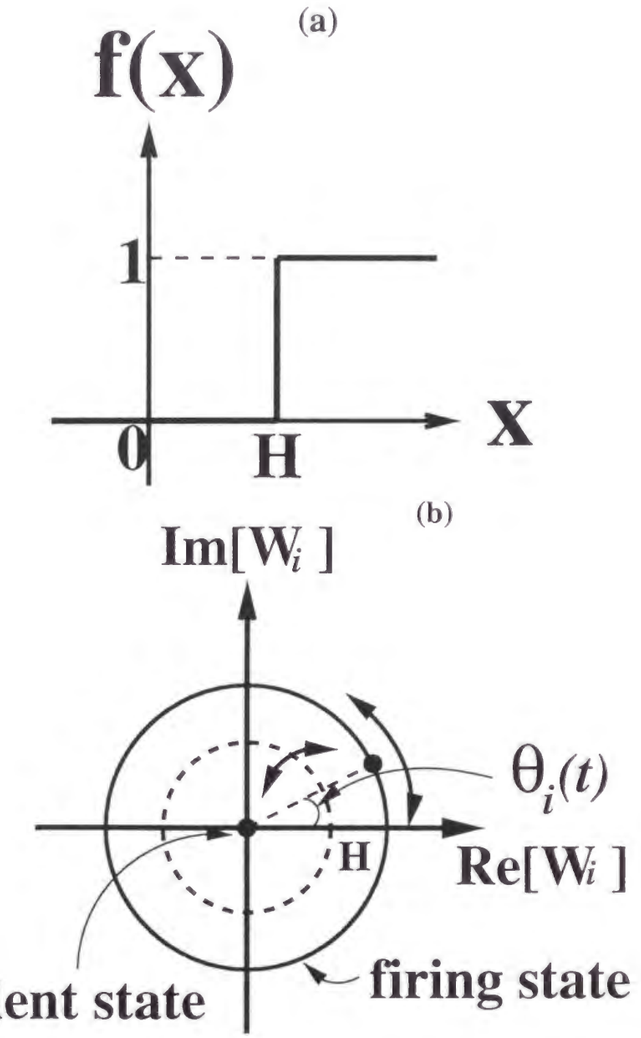


Figure 2.1: (a) The step function $f(x) = \Theta(x - H)$, where $H$ is the "threshold": When $|h_i(t)| \geq H$, $|W_i(t+1)| = 1$, and otherwise, $|W_i(t+1)| = 0$. (b) Depiction of the dynamical change of the state of the unit. The circle and the origin correspond to the firing state and the non-firing state, respectively. The phase and amplitude of $W_i(t)$ change according to Eq.(2.4).

(a)

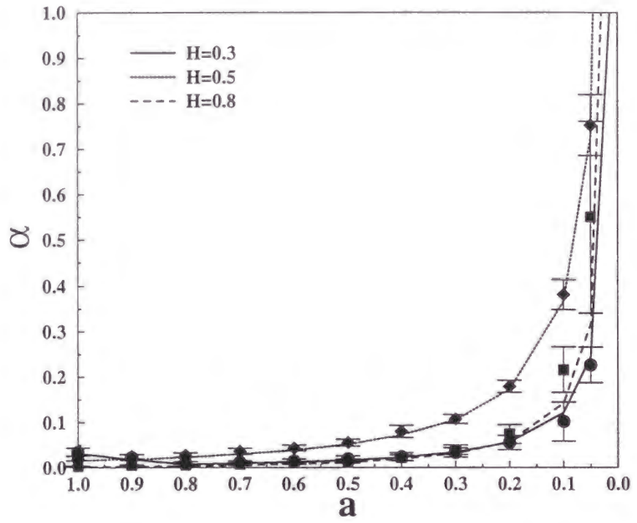


(b)

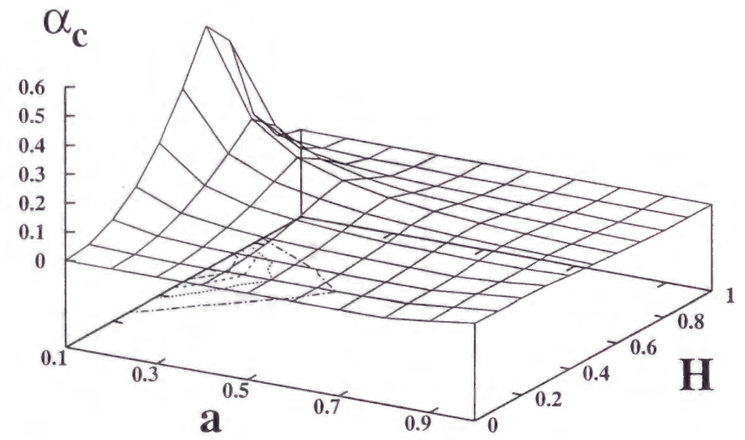


Figure 2.2: (a) Storage capacity $\alpha_c$ as a function of the mean activity level $a$ for various thresholds $H$. The data points indicate numerical results with $N = 1000$ for 20 trials. The lines were obtained from theoretical analysis. (b) A three-dimensional isometric plot of the maximum storage capacity $\alpha_c$ as a function of $a$ and $H$ from the theoretical results.



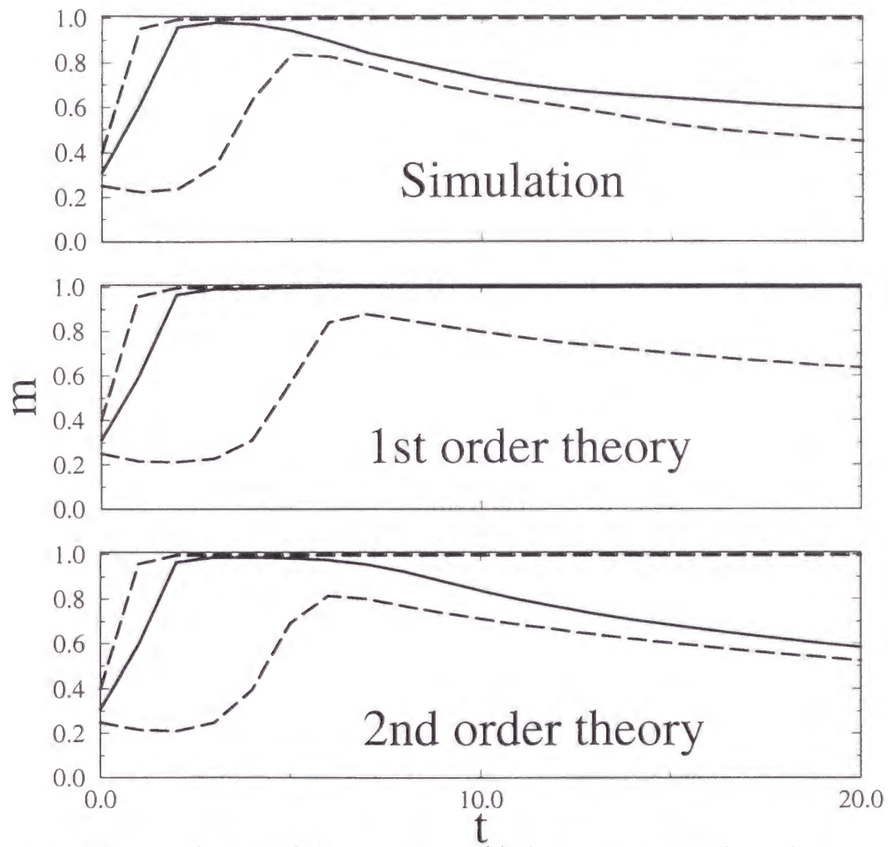


Figure 2.3: Time evolution of the overlap $m(t)$ for various initial conditions: $m = 0.25, 0.31, 0.4$. Here $\alpha = 0.013$, $H = 0.3$ and $a = 0.5$. Results of the second-order approximation give better agreement with the numerical simulation than those of the first-order approximation.

(a)

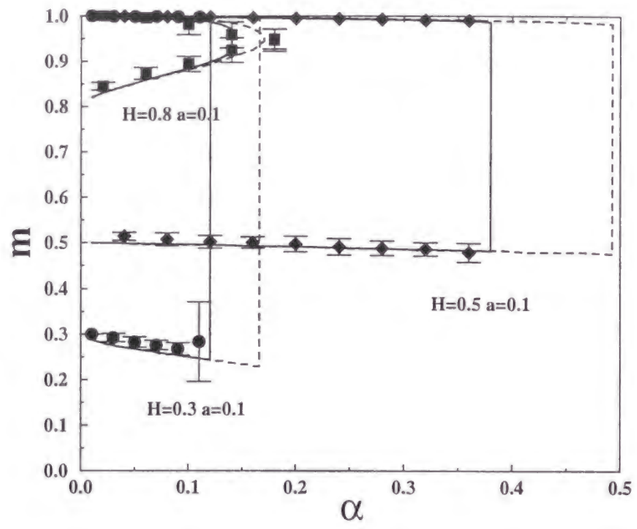


(b)

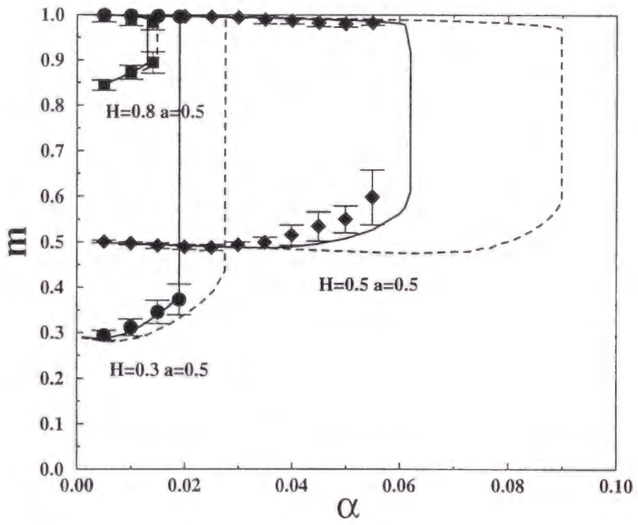


Figure 2.4: (a) Basins of attraction for various values of the threshold $H$, with $a = 0.1$. The data points are the results of the numerical simulation, the dashed lines correspond to the first-order approximation, and the solid lines correspond to the second-order approximation. The results of the numerical simulation were obtained with $N = 1000$ for 20 trials. (b) Same as (a) but with $a = 0.5$.



(a)

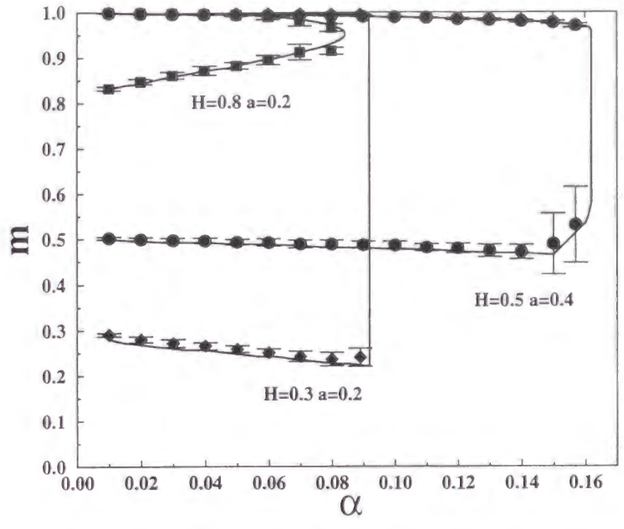


(b)

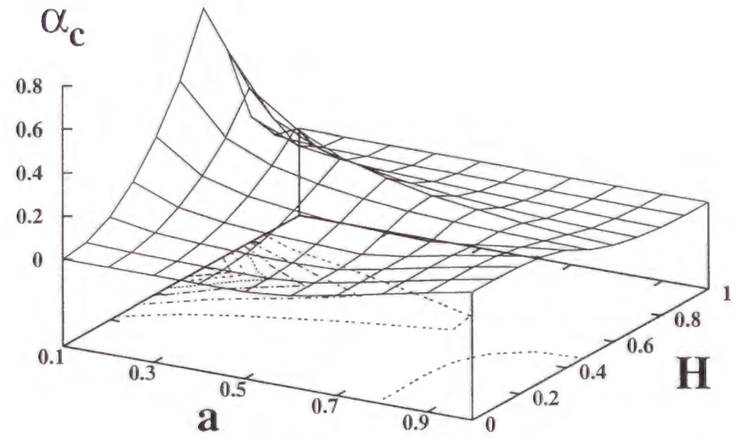


Figure 2.5: (a) Basins of attraction for various activity levels $a$ and thresholds $H$. The data points are the results of the numerical simulations ($N = 1000$ for 20 trials), and the solid lines are the theoretical results. (b) A three-dimensional isometric plot of the maximum storage capacity $\alpha_c$ as a function of $a$ and $H$ from the theoretical results.

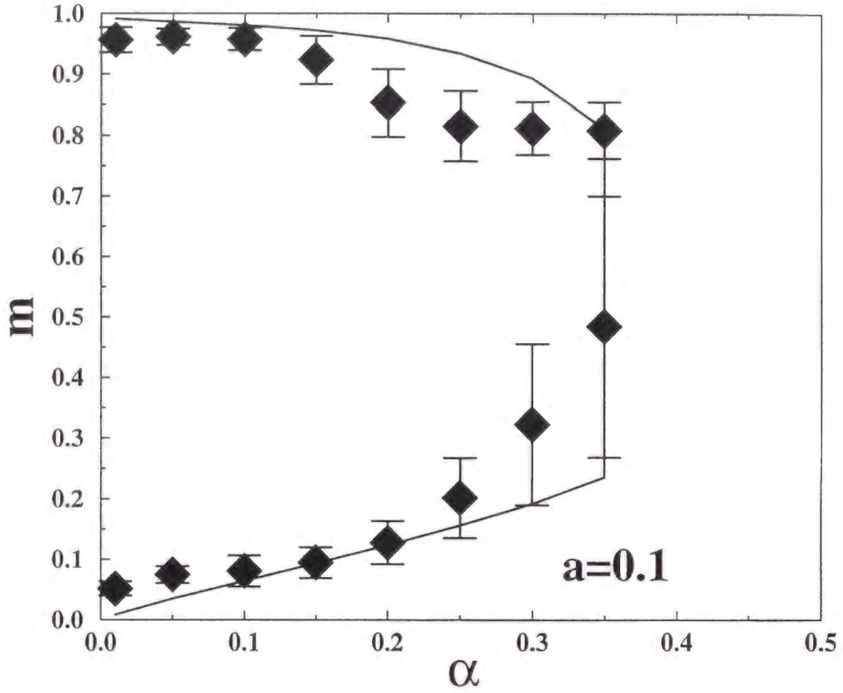


Figure 2.6: Basins of attraction in the case that $H(t)$ is a dynamically adjusted variable with $a = 0.1$. Comparing with Fig.2.4(a), we find that this mechanism enlarges the basin of attraction. The data points represent the results of a numerical simulation with $N = 1000$ for 20 trials, and the line is the theoretical result.



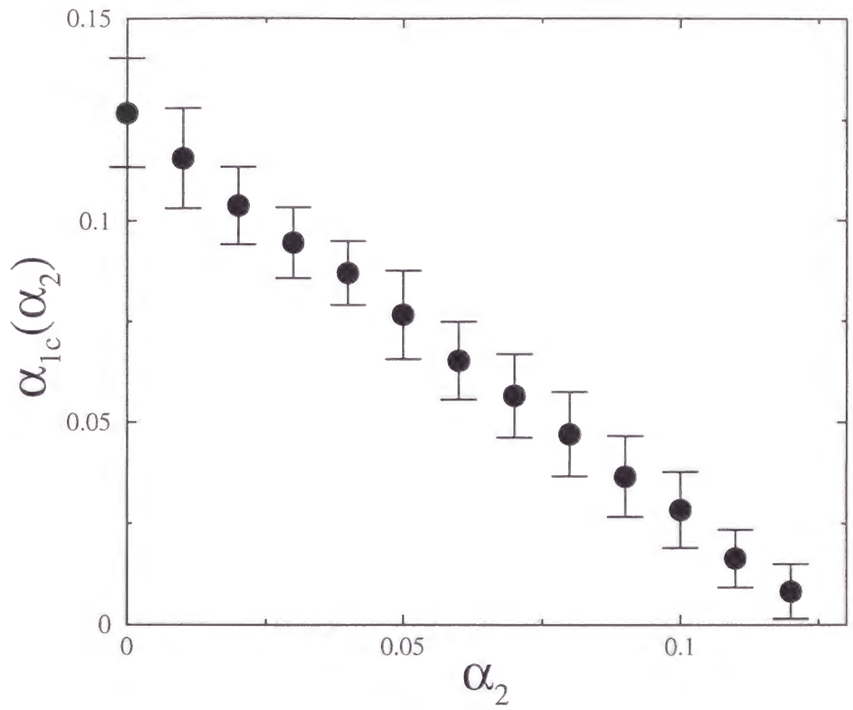


Figure 2.7: Storage capacity $\alpha_{1c}$ as a function of $\alpha_2$ for $a_1 = 0.1$ and $a_2 = 0.2$. The circular data points represent $\alpha_{1c}$ as a function of $\alpha_2$. We can see that $\alpha_{1c} + \alpha_2$ is constant. It was obtained from a numerical simulation with $N = 2000$ for 20 trials.

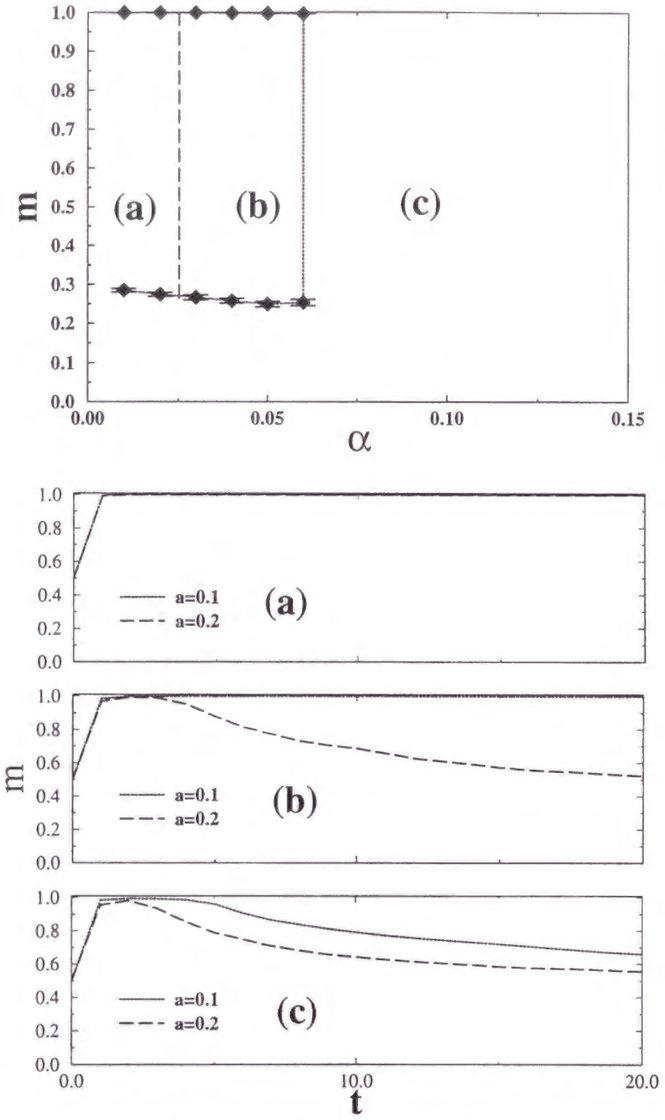


Figure 2.8: Top, basin of attraction for patterns with $a = 0.1$ in the case that patterns with $a = 0.1$ and $a = 0.2$ are embedded in equal number at the same time. Here $H = 0.3$. The dotted line and the data points represent the theoretical and the numerical results, respectively. The vertical long-dashed line indicates the maximum storage capacity for patterns with $a = 0.2$. Thus, in the left figure (a) is the region where both activity level patterns are successfully retrieved, (b) is the region where only patterns with $a = 0.1$ can be retrieved, and (c) is the region where neither can be retrieved. Bottom, time evolutions of the overlap $m(t)$ for the initial condition $m(0) = 0.5$, with $H = 0.3$ and $\alpha = 0.02, 0.05$ and 0.08, corresponding to the regions (a), (b) and (c) in the left figure, respectively. These are the results of the numerical simulation.



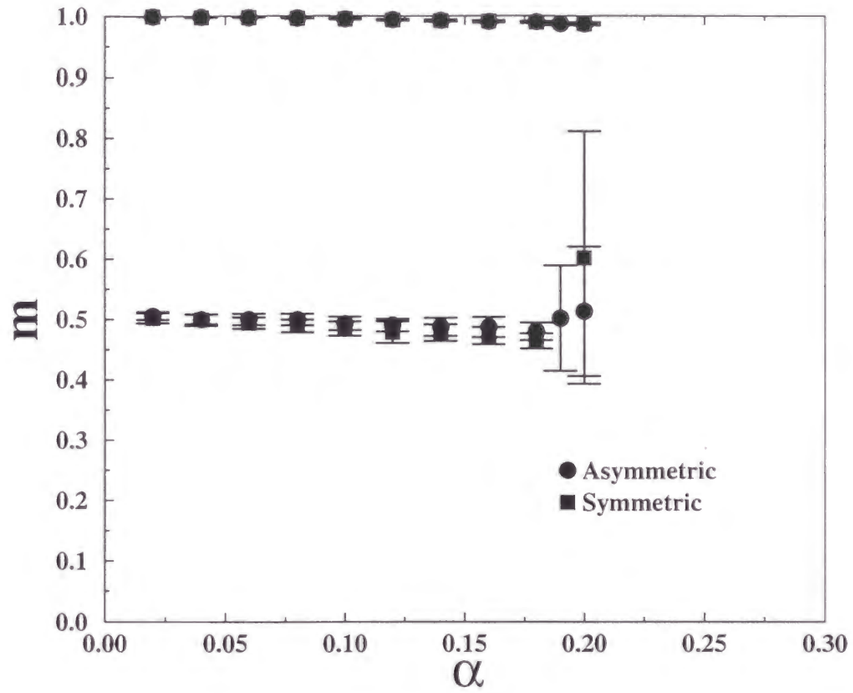


Figure 2.9: Comparison of basins for symmetrical and asymmetrical dilution. Both were obtained from numerical simulations with $N = 2000$ for 20 trials.

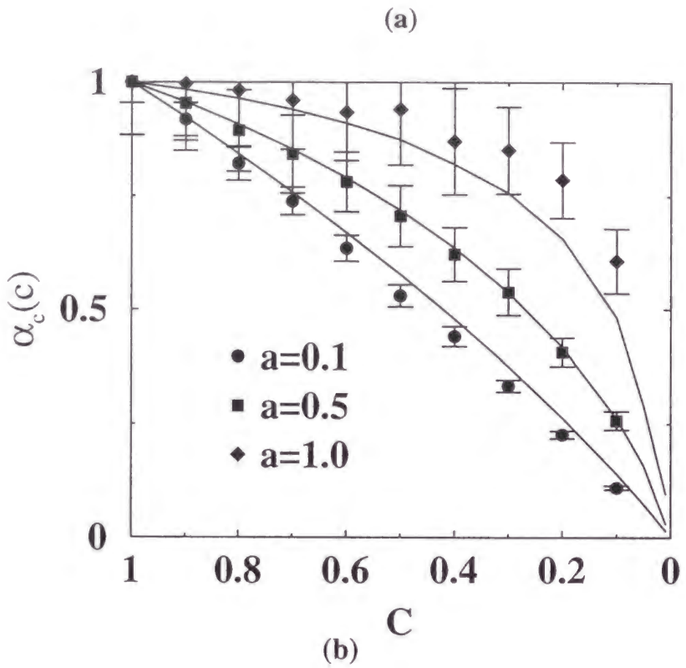


Figure 2.10: (a) Dependence of the maximum storage capacity on the ratio of connectivity $c$ for various activity levels with $H = 0.5$. Here we adopted the normalized maximum storage capacity by $\alpha_c(1)$. The solid lines represent the theoretical results, and the data points represent the numerical results with $N = 2000$ for 20 trials. (b) A three-dimensional isometric plot of the maximum storage capacity $\alpha_c$ as a function of $a$ and $c$ for $H = 0.5$. This was obtained from the theoretical results.



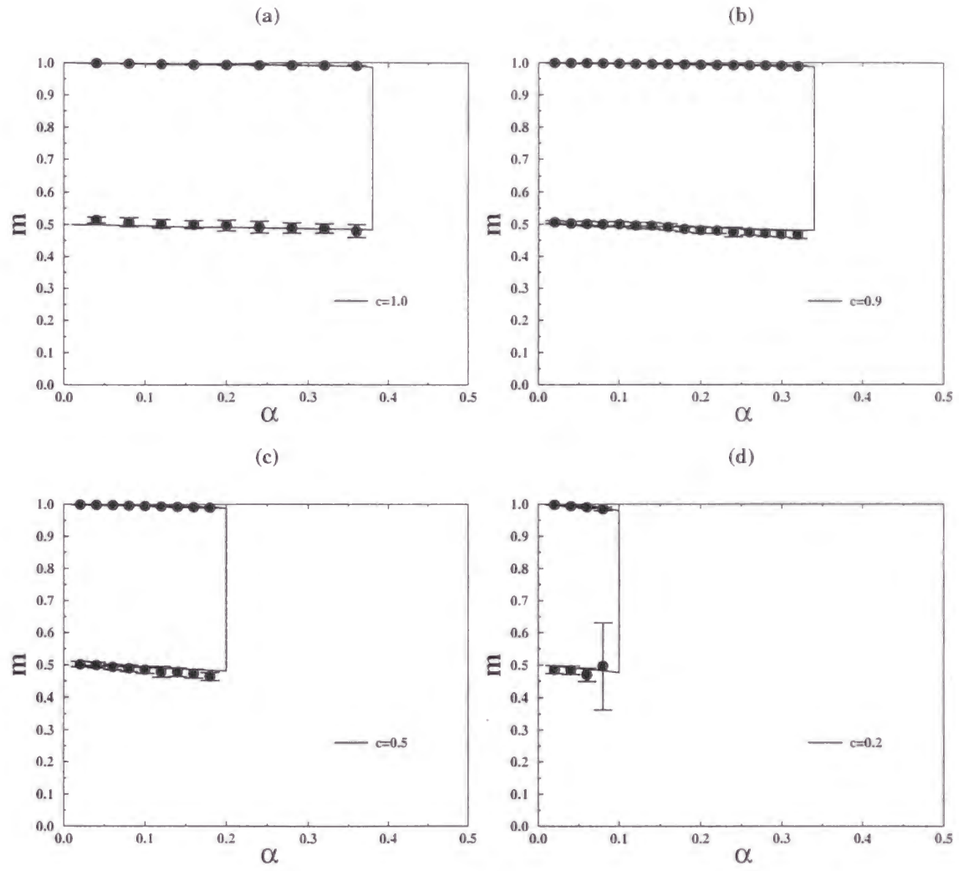


Figure 2.11: Basins of attraction for various values of the connectivity $c$. The solid lines represent the theoretical results, and the data points represent the numerical results with $N = 2000$ for 20 trials.

# Chapter 3

# Studies of Mixed States in Oscillator Neural Networks

## 3.1 Introduction

Through the studies of associative memory models with binary units, it is known that as a result of learning, a pattern, which is similar to learned patterns but not identical with them, becomes a stable state as illustrated in Fig.1.3. This state is called "mixed state" and theoretically studied with binary models [43, 44, 45]. Though we may consider it is unnecessary and undesirable for the information processing, some examples of using mixed states in the information processing have been reported [33, 34]. In addition, the physiological experiments by Miyashita [32] can be related to a mixed state.

For mixed states in the temporal cording, only a few study have been reported [35]. In this chapter, we study the mixed states on the oscillator model we have proposed in Chapter 2 except for patterns. We theoretically analyze the equilibrium state of the system and investigate the maximum storage capacity for the mixed state. In discussion, we propose a few examples applying the mixed states to the information processing.



## 3.2 Model

Following Chapter 2, we represent the state of the i-th unit and the local field produced by all other units at time $t$ by $W_i(t)$ and $h_i(t)$, respectively. Then we treat the following synchronous model:

$$W_i(t+1) = f(|h_i(t)|)\frac{h_i(t)}{|h_i(t)|}, \quad h_i(t) = \sum_{j=1}^{N} C_{ij} W_j(t), \tag{3.1}$$

where the effect of the interaction between the i-th and j-th units $C_{ij}$ is defined below.

Next, we define a set of complex patterns as follows:

$$\xi_i^{\mu\nu} = \eta_i^{\mu\nu} \exp(i\theta_i^{\mu}), (\mu = 1, \cdots, P; \nu = 1, \cdots, s; i = 1, \cdots, N), \tag{3.2}$$

where we choose $\eta_i^{\mu\nu}$ independently with the following probability distribution,

$$\eta_i^{\mu\nu} = \begin{cases} 1 & \text{for firing state with probability } a \\ 0 & \text{for silent state with probability } 1-a. \end{cases} \tag{3.3}$$

For the firing state, $\theta_i^{\mu}$ is chosen at random from a uniform distribution between 0 and $2\pi$.

With these patterns, we define two types of mixed states.

- Type 1: mixed state composed of patterns with the same phase

$$\chi_i^{\mu} = \Theta\left(\sum_{\nu=1}^{s} \eta_i^{\mu\nu} - 1\right) \exp(i\theta_i^{\mu}) \tag{3.4}$$

- Type 2: mixed state composed of patterns with the different phases

$$\chi_i = \Theta\left(\left|\sum_{\mu=1}^{P} \xi_i^{\mu 1}\right| - H\right) \frac{\sum_{\mu=1}^{P} \xi_i^{\mu 1}}{|\sum_{\mu=1}^{P} \xi_i^{\mu 1}|} \tag{3.5}$$

We illustrate examples of the original patterns and the mixed states in Fig.3.1. Figure3.1(a) and (b) correspond to the mixed state defined by Eq.(3.4) and (3.5), respectively. Note that the type 1 mixed state corresponds to the OR mixed state and we also

note that the mixed state defined by Eq.(3.5) is equivalent to that defined by Eq.(3.4) when all the phases at each site $\theta_i^\mu$ for $\mu = 1, ..., s$ are identical.

The original patterns defined by Eq.(3.2) and the mixed states defined by Eq.(3.4) organize the following a kind of hierarchical structure,

$$E[\xi_i^{\mu\nu}\tilde{\xi}_i^{\mu'\nu'}] = \begin{cases} 0 & (\mu \neq \mu') \\ a^2 & (\mu = \mu' \text{ and } \nu \neq \nu') \\ a & (\mu = \mu' \text{ and } \nu = \nu') \end{cases} \tag{3.6}$$

$$E[\chi_i^{\mu}\tilde{\xi}_i^{\mu'\nu'}] = \begin{cases} 0 & (\mu \neq \mu') \\ a & (\mu = \mu') \end{cases} \tag{3.7}$$

$$E[\chi_i^{\mu}\tilde{\chi}_i^{\mu'}] = \begin{cases} 0 & (\mu \neq \mu') \\ 1-(1-a)^s & (\mu = \mu'). \end{cases} \tag{3.8}$$

Figure 3.2 displays the structure between the original patterns and the type 1 mixed states.

Now, we define the effect of the interaction between the i-th and the j-th units with

$$C_{ij} = \begin{cases} \frac{1}{aN}\sum_{\mu=1}^{P}\sum_{\nu=1}^{s}\xi_i^{\mu\nu}\tilde{\xi}_j^{\mu\nu} & (i \neq j) \\ 0 & (i = j). \end{cases} \tag{3.9}$$

## 3.3 Theory

At first, we theoretically consider the stability of the type 1 mixed state defined in the system represented by Eq.(3.1), (3.2), (3.3) and (3.9). To analyze the equilibrium state of the system theoretically, we define the following order parameters. The storage capacity $\alpha$ is defined by $\alpha = sP/N$. And the overlap $m^{\mu\nu}(t)$ between $W_i(t)$ and $\xi_i^{\mu\nu}$ is defined by

$$m^{\mu\nu}(t) = |M^{\mu\nu}(t)| = \left|\frac{1}{aN}\sum_{j=1}^{N}\tilde{\xi}_j^{\mu\nu}W_j(t)\right|. \tag{3.10}$$

In addition, we define the overlap $m_m^\mu(t)$ between $W_i(t)$ and the mixed state $\chi_i^\mu$ by

$$m_m^\mu(t) = |M_m^\mu(t)| = \left|\frac{1}{a_m N}\sum_{j=1}^{N}\tilde{\chi}_j^{\mu}W_j(t)\right|, \tag{3.11}$$

where $a_m = 1-(1-a)^s$, which is the activity level of the mixed state.

In general, we can consider the situation in which the system is retrieving the mixed state



$\chi_i^1$, that is,

$$m^{1\nu}(t) \equiv m^\nu(t) \sim O(1), \quad m^{\mu\nu} \sim O\left(\frac{1}{\sqrt{N}}\right) \quad (\mu \neq 1) \tag{3.12}$$

$$m_m^1(t) \equiv m_m(t) \sim O(1), \quad m_m^\mu \sim O\left(\frac{1}{\sqrt{N}}\right) \quad (\mu \neq 1). \tag{3.13}$$

The local field $h_i(t)$ can be separated as

$$h_i(t) = \sum_{\nu=1}^{s} M^{1\nu}(t)\xi_i^{1\nu} + z_i(t), \tag{3.14}$$

where $z_i(t)$ is defined by

$$z_i(t) = \frac{1}{aN}\sum_{j=1}^{N}\sum_{\mu=2}^{P}\sum_{\nu=1}^{s}\xi_i^{\mu\nu}\tilde{\xi}_j^{\mu\nu}W_j(t). \tag{3.15}$$

We treat the second noise term as a complex Gaussian noise characterized by

$$E[z_i(t)] = 0, \quad E[|z_i(t)|^2] = 2\sigma^2(t). \tag{3.16}$$

Assuming the above, we obtain the equilibrium equations in the final form by applying the methods of statistical neurodynamics generalized to treat the structured patterns [46] (see appendix A),

$$m = \sum_{k=1}^{s} {}_{s-1}C_{k-1}a^{k-1}(1-a)^{s-k}\left\langle\left\langle f(|mk+z|)\frac{mk+z}{|mk+z|}\right\rangle\right\rangle_z, \tag{3.17}$$

$$m_m = \frac{1}{a_m}\sum_{k=1}^{s} {}_sC_k a^k(1-a)^{s-k}\left\langle\left\langle f(|mk+z|)\frac{mk+z}{|mk+z|}\right\rangle\right\rangle_z, \tag{3.18}$$

$$\sigma^2 = \frac{\alpha Q}{2s}\left[\left\{\frac{1+(s-1)a}{1-\{1+(s-1)a\}G}\right\}^2 + (s-1)\left\{\frac{1-a}{1-(1-a)G}\right\}^2\right], \tag{3.19}$$

$$G = \sum_{k=0}^{s} {}_sC_k a^k(1-a)^{s-k}\left\langle\left\langle\frac{f'(|mk+z|)}{2} + \frac{f(|mk+z|)}{2|mk+z|}\right\rangle\right\rangle_z, \tag{3.20}$$

$$Q = \sum_{k=0}^{s} {}_sC_k a^k(1-a)^{s-k}\left\langle\left\langle f^2(|mk+z|)\right\rangle\right\rangle_z. \tag{3.21}$$

## 3.4 The results

In Fig.3.3, we show the dependence of $\alpha_c$ on the activity level $a$ under the parameters $s = 1, 2, 3$ and $H = 0.5$. It shows that the maximum storage capacities concerning the mixed states ($s = 2, 3$) keep the feature similar to that of the maximum storage capacity concerning the embedded pattern itself ($s = 1$), that is, in the sparse coding limit $a \to 0$, the storage capacity diverges. Thus, we can conclude that the type 1 mixed state can be recalled stably.

Finally, we mention the stability of the type 2 mixed state. Figure3.4 displays the time dependence of the overlaps $m_m(t)$ ($s = 2$) of both the type 1 and the type 2 mixed state, which are calculated by the numerical simulations. It is shown that the type 2 mixed state could not be retrieved while the type 1 mixed state can be recalled successfully. We check this feature is seen in the several activity levels and/or $s$. This suggests that the type 2 mixed state is less stable than the type 1 mixed state.

## 3.5 Conclusion

In this study, we theoretically and numerically considered the stability of the mixed states in the extended oscillator neural network model. The results are summarized as follows.

- Applying the theory of statistical neurodynamics generalized for the structured patterns, we have estimated the maximum storage capacity of the type 1 mixed state. It suggests that the maximum storage capacity diverges in the sparse coding limit. Our theoretical results are in good agreement with numerical simulations.
- The numerical simulation suggests that the maximum storage capacity of the type 2 mixed state is less than that of the type 1 mixed state.

Based on these results, we mention following examples of using such mixed states in the information processing.



- Conformation of concept patterns

  It is said that we store memories in a hierarchical manner [32], and some papers modeling it have been proposed [47]. In addition, some authors have proposed models considering the relationship between the concept pattern and the mixed state [33]. Introducing the phase, we simply realize this function. Let us consider the following situation. We suppose the correlated patterns $\xi^{11}$ and $\xi^{12}$ to be the representations of the individuals in the category 1, and $\xi^{21}$ and $\xi^{22}$ to be the representations of the individuals in the category 2. In this situation, the mixed patterns $\chi^1$ and $\chi^2$ (see Fig.3.1(a)) can be considered as the concept patterns related to the category 1 and the category 2, respectively. These concept patterns are retrieved successfully. On the other hand, since the mixed state composed of $\xi^{11}$ and $\xi^{21}$ (see Fig.3.1(b)) is not so stable, we can say that few concept patterns are formed between them. In this sense, the phase and the amplitude represent the category and the individual, respectively.

  This is one of the examples showing the validity of using the timings of the spikes in the information processing, since with the traditional binary units, undesirable mixed states are also stable and successfully retrieved. This example realize the following conflicting situation.

  1. Usually, the memory patterns included in the same concept pattern should be similar to each other [33, 46].
  2. In some cases, each representation for physical property in the same concept might be different from others.
  3. On the other hand, representations for memory items belonging to different classes might share similar physical properties.

In this paper, we have treated homogeneous firing patterns which correspond to the homogeneous physical properties. The ultra-metric structure is only conveyed by the phase information of our model. This formulation corresponds to the situation that all of physical properties are homogeneous, and the concept information is only embedded in the phase information. It is the dual coding that enables this type of information processing.



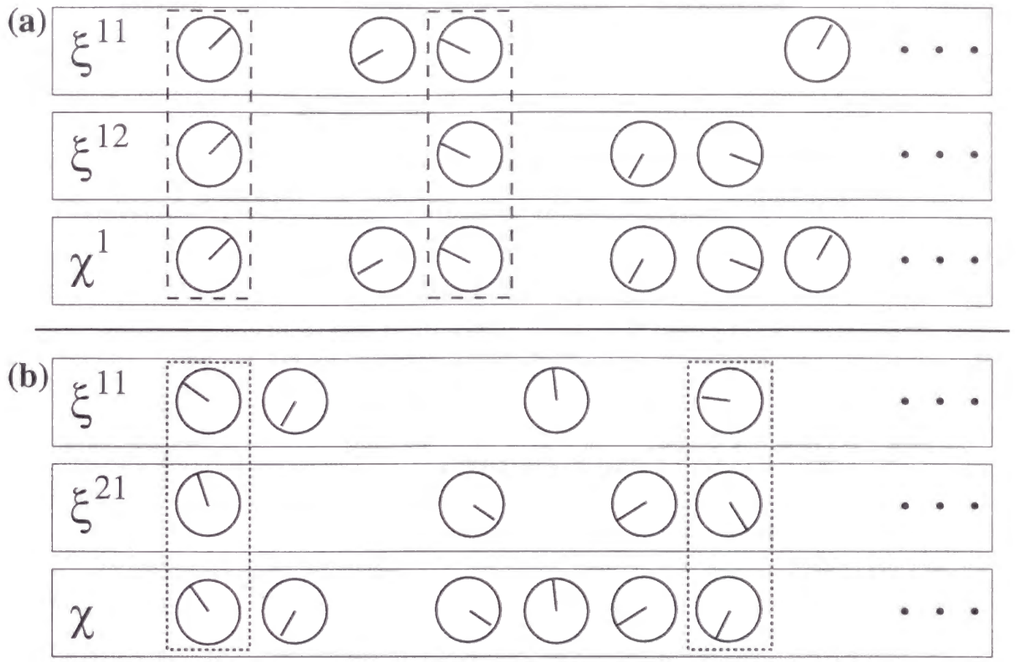


Figure 3.1: Depiction of the relationship between the embedded patterns and the mixed states for $s = 2$. The circles and the illustrated phases are correspond to the firing states and the timings of the spikes, respectively. (a) Type 1 mixed state: For the patterns such that the phases at the sites which fire simultaneously are identical (see the sites en closed with the long dashed squares), the mixed state could be considered to characterize the original patterns. (b) Type 2 mixed state: In contrast, when the phases are not identical (see the sites enclosed with the short dashed squares), the patterns may not organize a concept pattern.

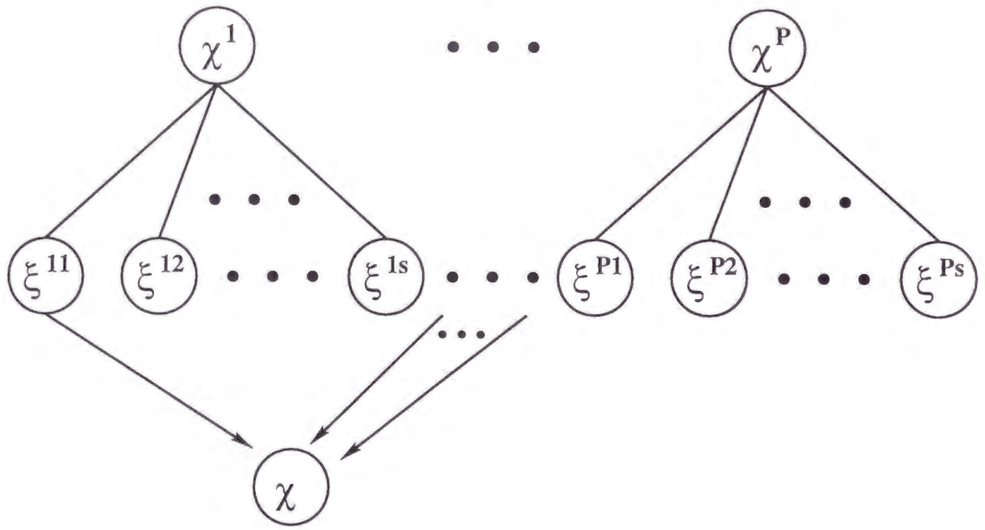


Figure 3.2: Depiction of the hierarchical structure between the type 1 mixed states and the original patterns. $\xi^{\mu\nu}$ and $\chi^{\mu}$ are the original patterns and the type 1 mixed states, respectively. Each phase pattern organizes the tree and the nodes belonging the same tree are correlated, however, there is no correlation among the nodes of different trees. The type 2 mixed state $\chi$ could not be classified into the structure.



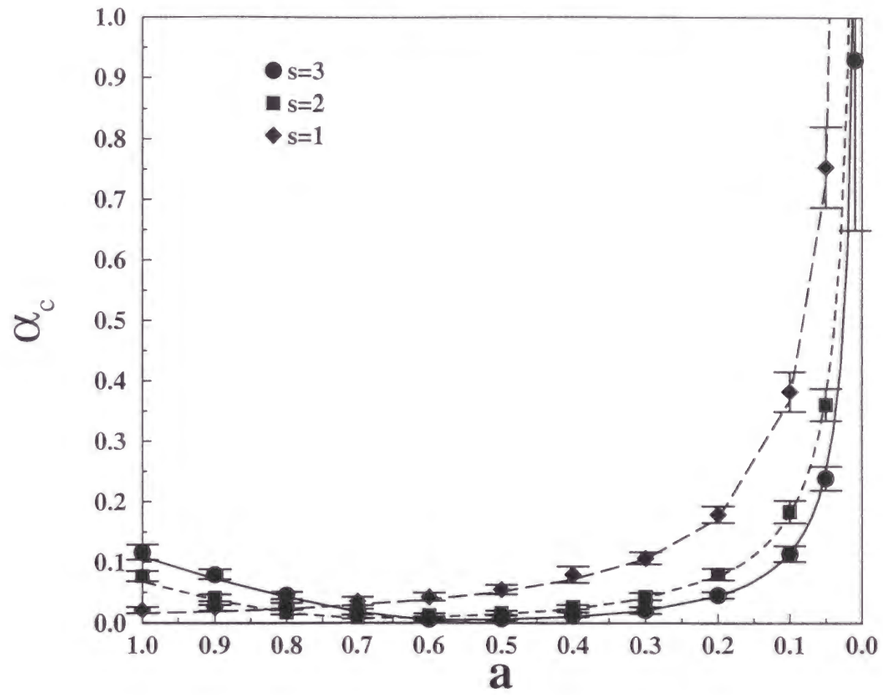


Figure 3.3: Storage capacity $\alpha_c$ as a function of the mean activity level $a$ for a threshold $H = 0.5$ and mixed numbers $s = 1, 2, 3$. The data points indicate numerical results with $N = 2000$ for 20 trials. The lines were obtained from theoretical analysis.

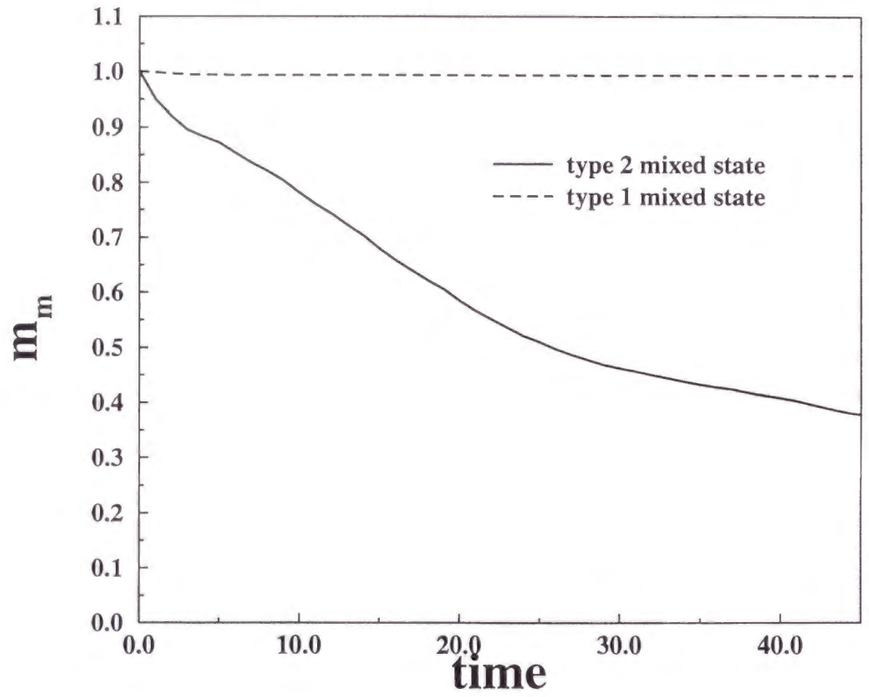


Figure 3.4: Time evolutions of the overlaps $m_m(t)$ of two types of the mixed states obtained from the numerical simulations. Here $s = 2$, $\alpha = 0.01$, $a = 0.5$ and $H = 0.5$. In this condition, the maximum storage capacity for the type 1 is approximately 0.14, thus, we can say that the type 2 mixed state is less stable than the type 1 mixed state .



# Chapter 4

# Conclusions

In the preceding chapters, we study the properties of the associative memory model with oscillator units under sparse coding. Here we summarize our results.

- The properties of the oscillator neural networks for sparsely coded phase patterns were studied. Here, we treated sparse coding and temporal coding at the same time. At first, applying the theory of statistical neurodynamics, we obtained the order parameter equations at the equilibrium state and those describing the retrieval process both in the auto-associative memory and in the sequence generator. From the equilibrium equations, it is found that the maximum storage capacity diverges in proportion to $-1/a \ln a$ in the sparse coding limit, as in the case of Hopfield model. From the dynamical equations, we estimated the basin of attraction, which seems narrow compared with the Hopfield model. However, we found that in auto-association, it can be enhanced by introducing the dynamically adjusted threshold. We also found theoretically that when the phase distribution in the embedded patterns is uniform, patterns with different activity levels can be memorized simultaneously, which can not be achieved in the Hopfield model. In addition, we theoretically investigated the robustness against the random synaptic dilution. It is found that even in a high cutting rate, the basin of attraction remains large, and the maximum storage capacity still diverges in the sparse coding limit. For low activity

patterns, the maximum storage capacity decreases almost linearly with the ratio of connected synapses. The validity of these theoretical results is confirmed by good agreement with numerical simulations.

- The stability of mixed states in the oscillator neural networks under sparse coding was studied. In this study, we adopted the correlated patterns to be memorized. Applying the methods of statistical neurodynamics, we theoretically investigated the maximum storage capacity concerning the OR mixed state, which is composed of patterns correlated each other. We found that it diverges in the sparse coding limit. The theoretical results are in good accordance with numerical simulations. Next, we compared the stability of the OR mixed state and that of the mixed state composed of uncorrelated patterns by numerical simulations. From the results, we can conjecture that the OR mixed state is more stable than the other type of mixed state. Using this difference of stability, we proposed an example of concept formation.

In this thesis, we found that introducing the timing of neuronal spikes causes new possibilities of information processing. In particular, the simple understanding of concept formation depends on the dual coding system. This coding mechanism gives us smart solutions for the binding problem.

Finally, we mention that although we treat only the coupled oscillator model in this thesis for the mathematical tractability, it is necessary to investigate properties of more realistic models such as Hodgkin-Huxley type for deeper understandings of real biological systems. We hope that our work will contribute the valuable knowledge to such future works.

# Bibliography


[1] P.Peretto, *An Introduction to the Modeling of Neural Networks* (Cambridge University Press, 1992).

[2] W.S.McCulloch and W.Pitts, *Mull.Math.Biophys.* **5**, *115* (1943).

[3] J.J.Hopfield, *Proc.Natl.Acad.Sci.USA* **79**, *2554* (1982).

[4] D.O.Hebb, *The Organization of Behavior* (Wiley, New York, 1949).

[5] D.J.Amit, H.Gutfreund and H.Sompolinsky, *Phys.Rev.Lett.* **55**, *1530* (1985).

[6] D.J.Amit, *Modeling Brain Function* (Cambridge University Press, 1989).

[7] S.Amari and K.Maginu, *Neural Netw.* **1**, *63* (1988).

[8] M.Abeles, *Local Cortical Circuits* (Springer-Verlag, Berlin, 1982).

[9] M.Okada, *Neural Netw.* **8**, *833* (1995).

[10] D.J.Willshaw, O.P.Buneman and H.C.Longuet-Higgins, *Nature* (London) **222**, *960* (1969).

[11] M.V.Tsodyks and M.V.Feigelman, *Europhys.Lett.* **6**, *101* (1988).

[12] C.J.P.Vicente and D.J.Amit, *J.Phys.A* **22**, *559* (1989).

[13] J.Buhmann, R.Divko and K.Schulten, *Phys.Rev.A* **39**, *2689* (1989).

[14] M.Okada, *Neural Netw.* **9**, *1429* (1996).

[15] E.Gardner, *J.Phys.A* **21**, *257* (1988).





[16] C.M.Gray, P.König, A.K.Engel and W.Singer, *Nature* (London) **338**, *334* (1989).

[17] C.M.Gray, *J.Comput.Neurosci.* **1**, *11* (1994).

[18] W.Singer, C.M.Gray, *Annu.Rev.Neurosci.* **18**, *555* (1995).

[19] W.Singer, A.K.Engel, A.K.Kreiter, M.H.J.Munk, S.Neuenschwander and P.R.Roelfsema, *Trens Cogn.Sci* **1**, *252* (1997).

[20] M.A.Arbib, P.Érdi and J.Szentágothai, *Neural Organization* (Cambridge, MA:MIT Press, 1997).

[21] G.Buzsáki, R.Llinás, W.Singer, A.Berthoz and Y.Christen, *Temporal Coding in the Brain* (Splinger, Berlin, 1994).

[22] C.von der Malsburg and W.Schneider, *Bio.Cybernet.* **54**, *29* (1986).

[23] H.Sompolinsky, D.Golomb and D.Kleinfeld, *Phys.Rev.A* **43**, *6990* (1991).

[24] D.Terman and D.L.Wang, *Physica* (Amsterdam) **81D**, *148* (1995).

[25] L.F.Abbot, *J.Phys.A* **23**, *3835* (1990).

[26] J.Cook, *J.Phys.A* **22**, *2057* (1989).

[27] A.J.Noest, *Europhys.Lett.* **6**, *469* (1988).

[28] T.Aoyagi and K.Kitano, *Neural Comput.* **10**, *1527* (1998).

[29] K.Kitano and T.Aoyagi, *Phys.Rev.E* **57**, *5914* (1998).

[30] T.Aoyagi, *Phys.Rev.Lett.* **74**, *4075* (1995).

[31] T.Aoyagi and K.Kitano, *Phys.Rev.E* **55**, *7424* (1997).

[32] Y.Miyashita, *Nature* **335**, *817* (1988).

[33] S.Amari, *Bio. Cyb.* **26**, *175* (1977).

[34] N.Parga and E.Rolls, *Neural Comput.* **10**, *1507* (1998).

[35] D.Wang, J.Buhmann, C.von der Malsburg, *Neural Comput.* **2**, *94* (1990).

[36] G.B.Erementrout and N.Kopell, *SIAM J.Math.Anal.* **15**, *215* (1984).

[37] Y.Kuramoto, *Chemical Oscillators, Waves, and Turbulence* (Springer, New York, 1984).

[38] H.Nishimori and T.Ozeki, *J.phys.A* **26**, *859* (1993).

[39] M.Shiino and T.Fukai, *J.Phys.A* **25**, *L375* (1992).

[40] A.C.C.Coolen and D.Sherrington, *Phys.Rev.Lett.* **71**, *3886* (1993).

[41] D.R.C.Dominguez and D.Bollé, *Phys.Rev.Lett.* **80**,*2961* (1998).

[42] H.Sompolinsky, *Phys.Rev.A* **34**,*2571* (1986)

[43] D.J.Amit, H.Gutfreund and H.Sompolinsky, *Phys.Rev.A* **32**, *1007* (1985).

[44] J.F.Fontanari, *Physique* **51**, *2421* (1990).

[45] T.Kimoto and M.Okada, *cond-matt/9911187* (1999).

[46] K.Toya, K.Fukushima, Y.Kabashima and M.Okada, *J.Phys.A* **33**, *2725* (2000).

[47] M.V.Feigelman, L.B.Ioffe, *Int.J.Mod.Phys.B* **1**, *51* (1987).

# Appendix A

# Derivation of Order Parameter Equations with Generalized Statistical Neuro Dynamics

From Eqs.(3.1), (3.10) and (3.14), $M^{1\nu}(t+1)$ $(\nu = 1, \cdots, s)$ is written by

$$\begin{aligned} M^{1\nu}(t+1) &= m^{\nu}(t+1)\exp(i\phi^{1\nu}(t+1)) = \frac{1}{aN}\sum_{j=1}^{N}\tilde{\xi}_j^{1\nu} f(|h_j(t)|)\frac{h_j(t)}{|h_j(t)|} \\ &= \frac{1}{aN}\sum_{j=1}^{N}\tilde{\xi}_j^{1\nu} f(|\sum_{\nu=1}^{s} M^{1\nu}(t)\xi_j^{1\nu} + z_j(t)|)\frac{\sum_{\nu=1}^{s} M^{1\nu}(t)\xi_j^{1\nu} + z_j(t)}{|\sum_{\nu=1}^{s} M^{1\nu}(t)\xi_j^{1\nu} + z_j(t)|}. \end{aligned}$$

Here we assume that the phase of $M^{1\nu}$ is almost constant, that is, $\phi^{1\nu}(t+1) = \phi^{1\nu}(t) \approx \phi_0$. Owing to the rotational symmetry of the complex Gaussian noise, $z_j(t)$ can be replaced with $z_j(t)\exp(i(\phi_0 + \theta_j^1))$. Doing so, the overlap is given by

$$m^{\nu}(t+1) = \frac{1}{aN}\sum_{j=1}^{N}\eta_j^{1\nu} f(|\sum_{\nu=1}^{s} m^{\nu}(t)\eta_j^{1\nu} + z_j(t)|)\frac{\sum_{\nu=1}^{s} m^{\nu}(t)\eta_j^{1\nu} + z_j(t)}{|\sum_{\nu=1}^{s} m^{\nu}(t)\eta_j^{1\nu} + z_j(t)|}. \tag{A.1}$$

Since we treat the symmetric mixed state, as far as the system successfully retrieves the mixed state, the overlaps are expected to keep the relation $m^{\nu}(t) \approx m(t)$ for all $\nu = 1, \cdots, s$. Applying this to Eq.(A.1), in the limit $N \to \infty$, we obtain

$$\begin{aligned} m(t+1) &= \frac{1}{aN}\sum_{j=1}^{N}\eta_j^{1\nu} f(|m(t)\sum_{\nu=1}^{s}\eta_j^{1\nu} + z_j(t)|)\frac{m(t)\sum_{\nu=1}^{s}\eta_j^{1\nu} + z_j(t)}{|m(t)\sum_{\nu=1}^{s}\eta_j^{1\nu} + z_j(t)|} \\ &= \sum_{k=1}^{s} {}_{s-1}C_{k-1}\, a^{k-1}(1-a)^{s-k}\left\langle\left\langle f(|m(t)k + z(t)|)\frac{m(t)k + z(t)}{|m(t)k + z(t)|}\right\rangle\right\rangle_{z(t)}. \end{aligned} \tag{A.2}$$



Similarly, the overlap $m_m(t+1)$ can be written by

$$m_m(t+1) = \frac{1}{1-(1-a)^s}\sum_{k=1}^{s} {}_sC_k\, a^k(1-a)^{s-k}\left\langle\left\langle f(|m(t)k + z(t)|)\frac{m(t)k + z(t)}{|m(t)k + z(t)|}\right\rangle\right\rangle_{z(t)}. \tag{A.3}$$

In the equilibrium state, $m(t+1) = m(t)$, $m_m(t+1)$, $z(t)$ can be replaced by $m$, $m_m$ and $z$, respectively. We now obtain Eqs.(3.17) and (3.18).

From Eq.(3.15), the noise at time $t+1$ is written by

$$z_i(t+1) = \sum_{\mu=2}^{P}\sum_{\nu=1}^{s}\xi_i^{\mu\nu} M^{\mu\nu}(t+1). \tag{A.4}$$

After this, we consider $M^{\mu\nu}(t+1)$ for $\mu = 2, \cdots, P; \nu = 1, \cdots, s$ in Eq.(A.4). It can be rewritten as follows,

$$\begin{aligned} M^{\mu\nu}(t+1) &= \frac{1}{aN}\sum_j \tilde{\xi}_j^{\mu\nu} W_j(t+1) \\ &= \frac{1}{aN}\sum_j \tilde{\xi}_j^{\mu\nu} f(|h_j(t)|)\frac{h_j(t)}{|h_j(t)|} \\ &= \frac{1}{aN}\sum_j \tilde{\xi}_j^{\mu\nu} f(|h_j^{-\mu}(t) + h_j^{\mu,-\nu}(t) + h_j^{\mu\nu}(t)|)\frac{h_j^{-\mu}(t) + h_j^{\mu,-\nu}(t) + h_j^{\mu\nu}(t)}{|h_j^{-\mu}(t) + h_j^{\mu,-\nu}(t) + h_j^{\mu\nu}(t)|}, \end{aligned} \tag{A.5}$$

where $h_j^{-\mu}(t)$, $h_j^{\mu,-\nu}(t)$ and $h_j^{\mu\nu}(t)$ are defined by

$$h_j^{-\mu}(t) = \frac{1}{aN}\sum_{k=1}^{N}\sum_{\alpha=2,\neq\mu}^{P}\sum_{\beta=1}^{s}\xi_j^{\alpha\beta}\tilde{\xi}_k^{\alpha\beta} W_k(t) \tag{A.6}$$

$$h_j^{\mu,-\nu}(t) = \frac{1}{aN}\sum_{k=1}^{N}\sum_{\beta=1,\neq\nu}^{s}\xi_j^{\mu\beta}\tilde{\xi}_k^{\mu\beta} W_k(t) \tag{A.7}$$

$$h_j^{\mu\nu}(t) = \frac{1}{aN}\sum_{k=1}^{N}\xi_j^{\mu\nu}\tilde{\xi}_k^{\mu\nu} W_k(t), \tag{A.8}$$

respectively. Note that these functions satisfy the relation $h_j(t) = h_j^{-\mu}(t) + h_j^{\mu,-\nu}(t) + h_j^{\mu\nu}(t)$. Since $h_j^{-\mu}$ is enough large compared with $h_j^{\mu,-\nu}(t) + h_j^{\mu\nu}(t)$, we can expand Eq.(A.5) with respect to $h_j^{-\mu}$. After that, carrying out the summation in Eq.(A.5) under the

assumption that $h_j^{-\mu}(t)$ is independent of $\xi_j^{\mu\nu}$, we obtain

$$M^{\mu\nu}(t+1) \sim \bar{M}^{\mu\nu}(t+1) + G(t)M^{\mu\nu}(t) + aG(t)\sum_{\beta=1,\neq\nu}^{s} M^{\mu\beta}(t), \tag{A.9}$$

$$\bar{M}^{\mu\nu}(t+1) = \frac{1}{aN}\sum_j \tilde{\xi}_j^{\mu\nu} f(|h_j(t)|)\frac{h_j(t)}{|h_j(t)|}, \tag{A.10}$$

$$G(t) = \sum_{k=0}^{s} {}_sC_k a^k (1-a)^{s-k} \left\langle\left\langle \frac{f'(|m(t)k+z(t)|)}{2} + \frac{f(|m(t)k+z(t)|)}{2|m(t)k+z(t)|}\right\rangle\right\rangle_{z(t)}, \tag{A.11}$$

where $f'$ means the derivative of $f$. Equation(A.9) can be rewritten in the vector form as

$$\mathbf{M}^\mu = \bar{\mathbf{M}}^\mu + G\mathbf{B}\mathbf{M}^\mu, \tag{A.12}$$

$$\mathbf{M}^\mu = (M^{\mu 1}, M^{\mu 2}, \cdots, M^{\mu s})^T, \tag{A.13}$$

$$\bar{\mathbf{M}}^\mu = (\bar{M}^{\mu 1}, \bar{M}^{\mu 2}, \cdots, \bar{M}^{\mu s})^T, \tag{A.14}$$

$$(\mathbf{B})_{\nu\nu'} = \delta_{\nu\nu'} + a(1-\delta_{\nu\nu'}), \tag{A.15}$$

where $\mathbf{B}$ is $s \times s$ matrix, and we neglect time $t+1$ and $t$ since we consider the equilibrium state. We can derive $\mathbf{M}^\mu$ from Eq.(A.12)

$$\mathbf{M}^\mu = (\mathbf{I} - G\mathbf{B})^{-1}\bar{\mathbf{M}}^\mu. \tag{A.16}$$

Equation(A.4) can be also rewritten in the following form

$$z_i = \sum_{\mu=2}^{P} \boldsymbol{\xi}_i^\mu (\mathbf{I} - G\mathbf{B})^{-1}\bar{\mathbf{M}}^\mu, \tag{A.17}$$

where $\boldsymbol{\xi}_i^\mu$ is defined by $\boldsymbol{\xi}_i^\mu = (\xi_i^{\mu 1}, \xi_i^{\mu 2}, \cdots, \xi_i^{\mu s})$. We can now calculate the variance $2\sigma^2$ from Eq.(A.17),

$$\begin{aligned} 2\sigma^2 &= \frac{1}{N}\sum_i |z_i|^2 \\ &= \frac{\alpha Q}{s} Tr\left(\mathbf{B}\left(\mathbf{I} - G\mathbf{B}\right)^{-1}\right)^2 \\ &= \frac{\alpha Q}{s}\sum_{\nu=1}^{s}\left(\frac{\lambda_\nu}{1-\lambda_\nu G}\right)^2, \end{aligned} \tag{A.18}$$

$$Q = \sum_{k=0}^{s} {}_sC_k a^k (1-a)^{s-k} \left\langle\left\langle f^2(|mk+z|)\right\rangle\right\rangle_z, \tag{A.19}$$



where $\lambda_\nu$ is the $\nu$-th eigenvalue of the matrix $\mathbf{B}$. Equation(A.18) leads to Eq.(3.19) by substituting the eigenvalues $\lambda_\nu$ into Eq.(A.18).

## List of publication


1. T. Aoyagi, and M. Nomura, Phys. Rev. Lett. **83**, *1062*, (1999).

   'Oscillator Neural Network Retrieving Sparsely Coded Phase Patterns'

2. M. Nomura and T. Aoyagi, J. Phys. A **33**, *8681*, (2000).

   'Analysis of oscillator neural networks for sparsely coded phase patterns'

3. M. Nomura, T. Aoyagi, and M.Okada, Neural Comput. (submitted).

   'Two-level hierarchy with sparsely and temporaly coded patterns and its possible functional role in information processing'